Classification and disk parameters of Herbig Ae/Be stars using WISE and AKARI data

Annapurni Subramaniam[1]* and B. Adara[2]

[1]*Indian Institute of Astrophysics, Koramangala, Bangalore 560 034, India*
[2]*Indian Institute of Science Education and Research, Trivandrum 695 016, India*

Abstract. We present the classification and disk parameters of 50 Herbig Ae/Be stars using WISE and AKARI data. These stars have been classified into 4 groups based on the scheme proposed by Koenig et al. (2012) using WISE pass bands and by constructing their SEDs using data up to 12 pass bands. We could successfully classify 18 sources as Class I, 22 as Class II, 6 as Class III and 4 as sources with transitional disk. One-third of the sample (classification of 14 of 50 and disk parameters of 19 of 50) were studied for the first time. SEDs created with and without AKARI data were found to be similar for a good fraction of sources, though some sources showed large deviation. The SEDs are also used to derive the stellar as well as the circumstellar disk parameters. Our analysis suggests that sources more massive than ∼ 6 $M_\odot$ may have a very short Class II phase. We have studied the correlation between various stellar and disk parameters. Among the present sample, this study tentatively suggests that one set of stars are found to lose their disk rapidly, within 3-4 Myr, whereas another set of sources are found to retain their disk as well as accretion till 6-8 Myr.

Keywords : HAeBe stars – classification – disk parameters – WISE, 2MASS and AKARI surveys

1. Introduction

Herbig Ae/Be (HAeBe) stars are intermediate mass pre-main sequence (PMS) stars, found to possess a natal accretion disk which is a remnant of star formation Hillenbrand et al. (1992). Herbig (1960) first classified 26 stars of A and B spectral type as HAeBe which showed emission in Balmer lines and which were associated with nebulosity. Later more HAeBe stars were

---

*e-mail: purni@iiap.res.in

discovered by Finkenzeller & Mundt(1984), Herbig & Bell (1988) and Thé et al. (1994). From the IRAS all-sky far-infrared survey, several HAeBe stars were found not to be associated with active star formation region (with nebulosity). Hence the definition for HAeBe stars got modified as stars of A and B spectral type with emission lines, Infrared excess due to circumstellar dust and which belongs in the luminosity class III to V (Waters & Waelkens 1998, van den Ancker et al. 1997).

HAeBe stars are the most massive objects to experience an optically visible pre-main sequence phase, bridging the transition between low- and high-mass stars. Although these are highly interesting objects, our knowledge about the properties of the HAeBe regime is much more limited than that for the T Tauri stars (Mendigutía et al. 2012). The main reason is the comparatively smaller HAeBe sample, caused by the faster evolution of massive stars to the main-sequence, and by the fact that star formation favours lower mass objects, as the shape of the initial-mass function suggests.

The HAeBe stars have not been studied so far using the WISE data, along with the 2MASS data. As this combination measures flux from 1 - 22 μm, properties of the star and the circumstellar material can be estimated accurately. We have also combined the AKARI data, which covers the wavelength range, 50 - 180 μm, which further samples the cooler disk. Recently, Huang et al. (2013) studied a test sample of Herbig Ae/Be stars and classical T Tauri stars, where they were cross-identified with the 2MASS and AKARI catalogs to define the loci of YSOs with different masses on the color-color diagrams. Well classified Class I and Class II sources were taken as a second test sample to discriminate between various types of YSOs at possibly different evolutionary stages.

Clearing of the inner parts of the disk by photo evaporation by the star or by planet formation produces stars that exhibit excess emission only at wavelengths > 20μm, the so-called transition disks. The absence or low level of excess emission from 1 to 10μm and large excess beyond 20μm has been modeled as arising from a truncated optically thick outer disk and a dissipated inner disk or a radial gap in the inner disk (for example, Calvet et al. 2005; D'Alessio et al. 2005). These transition disks may be created by binary systems; however, recent work by Pott et al. (2010) has shown that these may be rare occurrences and planet formation or brown dwarf companions may be responsible for the inner disk clearing (Andrews et al. 2011). The ages of transition disks are uncertain. Giant planet formation may be able to produce disk clearing on timescales <5 Myr, as photo evaporation of the disk may take a longer time to operate (for example, Alexander & Armitage 2009). Inclusion of WISE and AKARI data along with the 2MASS data in this study will help to identify the presence of transition disk objects in the sample studied.

Hernandez et al. (2004) performed spectral analysis and classification of 75 early type emission line stars. The paper provides data on visual magnitude, distance, temperature, extinction etc of 58 early type emission line stars, among those 39 are identified as HAeBe stars (their Table 2). Others were found to have undefined evolutionary status and insufficient data. Thus, a good fraction of the stars requires classification. In this study, we have included the near-infrared (NIR) and mid-infrared (MIR) data of this sample of stars. We have used the NIR data from the 2MASS

Table 1. Table of magnitudes and respective errors from 2MASS (J, H, K_s) and WISE (W1, W2, W3, W4) used for the classification.

No	Name	V	J	eJ	H	eH	K	eK	W1	eW1	W2	eW2	W3	eW3	W4	eW4
1	V633 Cas	14.18	9.988	0.031	7.889	0.029	6.290	0.016	5.282	0.072	4.123	0.038	1.230	0.020	5.033	99.99
2	LkHα 201	13.64	10.716	0.024	10.285	0.031	9.849	0.022	9.306	0.023	8.922	0.020	8.077	0.025	7.059	0.068
3	AB Aur	7.05	5.936	0.018	5.062	0.020	4.230	0.016	3.254	0.135	2.142	0.082	0.682	0.009	-1.713	0.004
4	T Ori	10.63	8.271	0.021	7.236	0.047	6.216	0.023	5.252	0.059	4.395	0.039	2.517	0.037	0.227	0.025
5	PQ Tau	12.63	10.558	0.020	9.857	0.016	9.696	0.019	9.572	0.023	9.529	0.021	9.661	0.420	6.580	0.005
6	RR Tau	12.08	9.685	0.020	8.416	0.016	7.389	0.023	6.026	0.046	5.334	0.032	3.601	0.015	1.717	0.016
7	HD 250550	9.54	8.475	0.020	7.528	0.026	6.635	0.018	5.634	0.057	4.633	0.039	2.420	0.010	0.046	0.015
8	LkHα 208	11.65	10.254	0.020	9.834	0.023	9.245	0.021	7.931	0.023	6.613	0.023	2.538	0.015	0.762	0.017
9	LkHα 338	15.12	11.274	0.023	10.065	0.022	8.615	0.019	6.601	0.041	5.261	0.027	2.536	0.017	0.404	0.013
10	LkHα 339	13.66	11.386	0.023	10.640	0.022	9.725	0.019	8.179	0.023	7.242	0.018	3.677	0.015	1.369	0.019
11	LkHα 341	13.39	9.374	0.027	8.439	0.042	8.071	0.034	7.796	0.027	7.629	0.023	7.313	0.021	6.793	0.087
12	V590 Mon	12.77	11.438	0.024	10.448	0.024	9.330	0.028	7.864	0.025	6.919	0.020	2.957	0.015	0.614	0.021
13	V360 Mon	13.39	11.636	0.024	11.015	0.023	10.551	0.019	10.214	0.025	9.857	0.023	7.398	0.022	5.362	0.104
14	LkHα 118	11.20	8.721	0.020	8.248	0.047	7.900	0.023	7.377	0.025	7.113	0.020	6.584	0.029	5.195	0.005
15	VV Ser	11.92	8.673	0.020	7.435	0.057	6.321	0.020	5.194	0.076	3.914	0.056	2.386	0.010	0.980	0.019
16	AS 310 NW	12.45	11.641	0.005	13.171	0.264	11.712	0.115	7.271	0.022	6.335	0.021	0.091	0.060	-2.831	0.033
17	PX Vul	11.49	9.324	0.020	8.546	0.024	7.910	0.018	6.882	0.029	6.411	0.021	4.759	0.014	2.743	0.020
18	V751 Cyg	14.18	16.012	0.106	14.643	0.075	14.106	0.067	13.677	0.037	13.514	0.052	10.739	0.164	7.685	0.176
19	LkHα 324	12.61	10.020	99.99	9.815	0.017	9.574	0.108	8.825	0.016	8.215	0.014	4.183	0.013	1.924	0.021
20	LkHα 349	13.37	9.639	0.021	8.908	0.044	8.589	0.021	8.303	0.023	8.144	0.017	8.557	0.282	7.056	0.191
21	LkHα 234	12.21	9.528	0.019	8.201	0.023	7.081	0.018	4.977	0.061	3.546	0.042	1.851	0.029	-1.636	0.008
22	BD +46° 3471	9.89	8.540	0.021	8.020	99.99	7.219	0.005	5.611	0.058	4.532	0.039	3.489	0.014	2.006	0.016
23	LkHα 233	13.56	11.294	0.032	10.307	0.029	8.921	0.020	6.540	0.040	4.926	0.035	2.302	0.009	-0.639	0.007
24	LkHα 314	14.04	10.765	0.023	9.844	0.022	8.963	0.021	6.847	0.034	5.597	0.025	3.227	0.012	1.045	0.014
25	MC1	10.77	12.920	0.026	12.014	0.031	11.004	0.025	9.002	0.023	7.656	0.020	4.153	0.014	1.430	0.014
26	VX Cas	11.28	10.145	0.022	9.171	0.028	8.214	0.018	7.140	0.033	6.587	0.020	4.158	0.014	1.834	0.015
27	RNO 6	14.52	12.272	0.031	11.789	0.041	11.419	0.035	9.963	0.025	9.224	0.021	4.808	0.016	2.486	0.027
28	IP Per	10.47	9.139	0.020	8.409	0.018	7.589	0.016	6.592	0.041	6.111	0.022	5.192	0.015	2.243	0.019
29	XY Per EW	9.21	7.654	0.018	6.917	0.017	6.092	0.018	4.922	0.076	3.786	0.058	2.546	0.012	0.973	0.016
30	V892 Tau	15.25	8.742	0.027	7.016	0.029	5.787	0.016	5.101	0.066	3.856	0.051	-0.414	0.016	-2.557	0.001
31	UX Ori	10.40	8.707	0.021	8.044	0.034	7.214	0.020	6.242	0.046	5.511	0.032	2.923	0.013	0.923	0.012
32	RY Tau	11.80	7.155	0.019	6.128	0.061	5.395	0.023	4.237	0.088	3.150	0.068	0.990	0.027	-0.860	0.015
33	P1394	10.13	8.993	0.026	8.628	0.071	8.279	0.027	7.652	0.026	7.121	0.022	3.855	0.013	1.689	0.020
34	HD 245185	9.89	9.291	0.030	8.764	0.053	8.020	0.036	6.920	0.036	6.225	0.021	2.521	0.011	0.515	0.018
35	CQ Tau	10.27	7.926	0.023	7.060	0.024	6.173	0.018	5.317	0.069	4.318	0.039	1.837	0.007	-0.793	0.007
36	BN Ori	9.67	8.604	0.024	8.371	0.036	8.231	0.024	8.181	0.024	8.185	0.021	8.177	0.026	8.244	0.005
37	BD +26° 887	10.47	9.134	0.021	8.507	0.031	7.976	0.026	7.318	0.028	6.895	0.021	4.555	0.015	2.398	0.017
38	V350 Ori	11.47	10.017	0.024	9.236	0.027	8.371	0.023	7.348	0.028	6.787	0.019	4.322	0.013	2.128	0.015
39	LkHα 215	10.54	8.598	0.029	7.821	0.044	7.034	0.016	5.893	0.045	4.840	0.031	2.985	0.014	0.782	0.023
40	HD 259431	8.73	7.454	0.026	6.666	0.034	5.726	0.020	4.425	0.087	3.169	0.074	1.143	0.019	-0.757	0.013
41	VSB2	13.33	11.811	0.026	11.403	0.023	11.315	0.023	11.226	0.024	11.229	0.022	10.651	0.145	8.679	0.529
42	W121	10.80	10.783	0.022	10.306	0.024	10.206	0.025	10.116	0.027	10.117	0.024	8.478	0.005	5.861	0.005
43	LkHα 218	11.87	10.255	0.023	9.419	0.022	8.577	0.024	7.306	0.027	6.428	0.019	3.904	0.016	2.207	0.023
44	WW Vul	10.74	9.092	0.030	8.181	0.042	7.278	0.017	6.579	0.035	5.947	0.024	3.325	0.013	1.558	0.016
45	V1685 Cyg	10.69	7.904	0.023	6.792	0.018	5.766	0.016	4.226	0.018	2.879	0.027	0.407	0.036	-1.284	0.015
46	LkHα 147	14.46	10.565	0.024	9.997	0.032	9.483	0.024	8.950	0.023	8.559	0.020	7.616	0.022	6.267	0.065
47	BD +65° 1637	10.18	8.973	0.020	8.729	0.024	8.474	0.020	7.905	0.023	7.495	0.020	5.013	0.019	0.233	0.015
48	BH Cep	11.16	9.686	0.025	8.993	0.030	8.310	0.023	7.326	0.030	6.837	0.019	4.681	0.015	2.219	0.014
49	BO Cep	11.60	10.319	0.024	9.849	0.028	9.581	0.024	8.932	0.022	8.612	0.019	7.026	0.015	3.861	0.020
50	SV Cep	10.98	79.350	0.035	8.560	0.047	7.744	0.021	6.742	0.037	5.978	0.022	2.554	0.010	0.746	0.013

catalog and MIR data from the WISE and AKARI catalogs. The classification used in this study is that prescribed by Koenig et al. (2012), using WISE data, which is tied up to the classification developed for Spitzer data. A good number of HAeBe stars from this sample are already classified as mentioned earlier, on the other hand, about one third of the sample is unclassified. We not only attempt to classify these unclassified objects based on their location in the diagnostic colour-colour diagnostic diagrams, but also check and confirm the classification of other stars. In this study, the YSOs are classified into the canonical categories of Class I YSOs (protostars with infalling envelopes, including flat spectrum objects) and Class II YSOs (pre-main-sequence stars with optically thick disks), Class III sources (diskless pre-main sequence stars which lack infrared excess) and sources with transition disks. 2MASS, WISE and AKARI data are combined for the first time to study the HAeBe stars. Using the multi-wavelength data (up to 12 pass bands), we constructed the SEDs using Robitaille et al. (2007) models. We estimated the physical properties such as mass, age, mass and accretion rate of disks of the HAeBe stars and explore correlation among these parameters.

The paper is arranged as follows. Section 2 gives the details of the data used. Section 3 presents the classification based on WISE colours, section 4 presents classification based on SED. Section 5 presents the estimation of star and disk parameters, section 6 presents the discussion, followed by conclusion in Section 7.

2. Data

The Wide field Infrared Survey Explorer, (WISE) mapped the entire sky simultaneously in four infrared (IR) bands centered at 3.4μm, 4.6μm, 12μm and 22 μm wavelength bands (W1, W2, W3, and W4, respectively). The WISE catalog as well as images are available from the WISE data archive and we make use of these in this study. The WISE catalog provides a merged catalog with the 2MASS catalog, thus we have magnitudes in 3 NIR and 4 MIR bands. We were able to compile reliable magnitude estimations, only for 50 sources. Estimations with error in magnitude less than 0.1 mag are taken, except in a few cases. In Table 1 we list the compiled magnitudes of 50 HAeBe stars in the above 7 pass bands along with the V magnitude taken from Hernandez et al. (2004). The WISE point spread function, full width at half-maximum in bands W1 to W4 are 6.1″, 6.4″, 6.5″, and 12.0″ respectively (Wright et al. 2010). WISE has poorer spatial resolution when compared to the 2MASS catalog, which is about 2″. Since the WISE catalog is already merged with the 2MASS catalog, we assume that there is very little source confusion.

We have also used the Bright star catalog of AKARI (Yamamura et al. 2010) to compile fluxes of HAeBe stars. The Far-Infrared surveyor has 4 pass bands centered at 65, 90, 140, and 160μm and the source catalog has a resolution of 48″ and a positional accuracy of 2.5″. The WISE and AKARI data are cross-correlated and matches are found within a radius of 2.5″. As the spatial resolution of AKARI is poorer than WISE, there is a possibility that the measured flux in AKARI pass bands might also include flux from sources near HAeBe stars, in dense environments of star forming regions. As there could be more flux in these pass bands, we first

compute SEDs without AKARI data and then with AKARI data. We analyse case by case and discuss whether AKARI data is reliable or not.

3. Classification based on WISE colour-colour diagram

The stars have been classified into 4 groups based on the scheme proposed by Koenig et al. (2012). We have shown the ([W2]−[W3]) versus ([W1]−[W2]) colour-colour diagram in Fig. 1 and ([W2]−[W4]) versus ([W1]−[W2]) color-color diagrams in Fig. 2. For easy identification, we have shown the identification number of the star in the figures. Koenig et al. (2012) classified stars in to class I, class II, class III/diskless stars and stars with transition disk based on their location in the above diagnostic diagrams, which was developed based on the regions occupied by known (already classified) sources. Based on these diagrams, we have classified the HAeBe stars in to 4 groups. In Fig. 1, the top most box encloses most of the Class I sources. The box below shows the location of Class II sources, though sources redder than 3.0 in ([W2]−[W3]) colour are not classified as Class II. The bottom most box shows the location of Class III sources. In Fig. 2, the top most box shows the location of Class I sources and the bottom area shows the location of transition disk objects. The area in between is occupied by the Class II objects. In both the figures, object 16 (AS 310 MW) is found to be located outside the figure boundaries. In order to compare the location of these stars in the NIR colour-colour diagram, we have shown the reddening corrected $(H-K)_0$ vs $(J-H)_0$ diagram in Fig. 3. We have used the extinction (A_V) given in Hernandez et al. (2004) to correct for reddening. The reddening $E(B-V)$ is derived from A_V using a value of 3.1 for R_V. The reddening relations are taken from Bessel & Brett (1988) and the following relations are used.

$$E(J - H) = 0.37 * E(B - V)$$
$$E(H - K) = 0.19 * E(B - V)$$

We have discussed each class below with details on our classification and comparison with the literature classification. It should be noted that the classification scheme used here is based on NIR and MIR flux. The circumstellar material is sampled well in this region of the IR and the scheme is derived based on Spitzer pass bands and extended to WISE pass bands. Also, we have attempted classification based on homogeneous data. This classification allows to identify objects with transition disks among the sample studied here. The other classification in the literature are discussed below. The classification by Hillenbrand et al. (1992) is based on SEDs, Fuente et al. (2002) is based on molecular lines and continuum emission at millimeter wavelengths, Verhoeff et al. (2012) is based on N-band imaging and long-slit spectroscopic data and Mendigutía et al. (2012) is based on optical to mid IR SEDs.

3.1 Class I sources

Class I stars are thought to be protostars with infalling envelope. Based on the location in Figs 1 and 2, we arrive at the following conclusions. Among the class I stars, the classification for
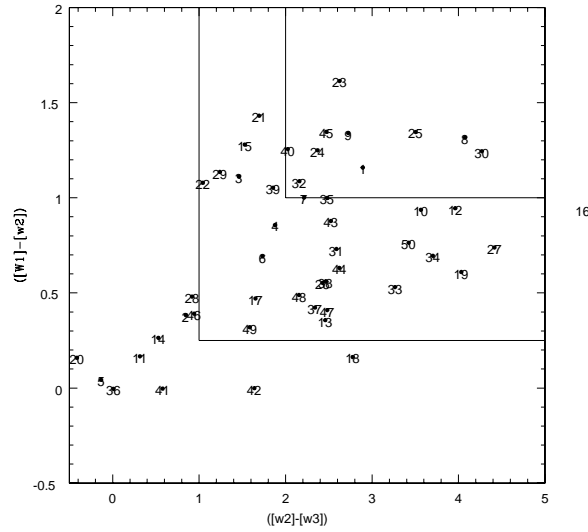
Figure 1. The ([W2]−[W3]) vs ([W1]−[W2]) colour-colour using the WISE pass bands. For easy identification, we have shown the identification number of the star in the figure.
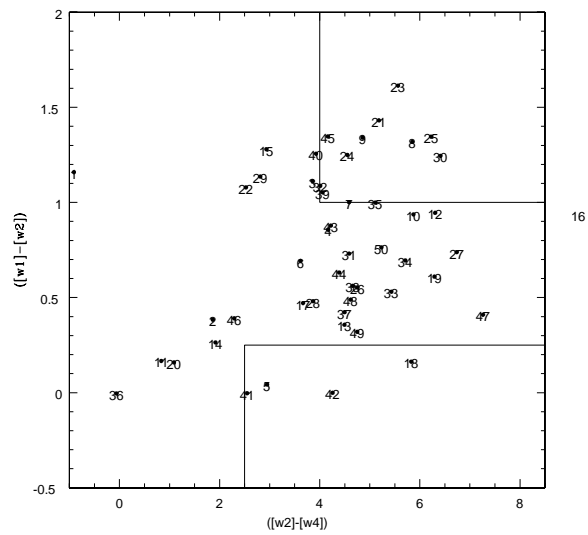
Figure 2. The ([W2]−[W4]) vs ([W1]−[W2]) colour-colour using the WISE pass bands. For easy identification, we have shown the identification number of the star in the figure.
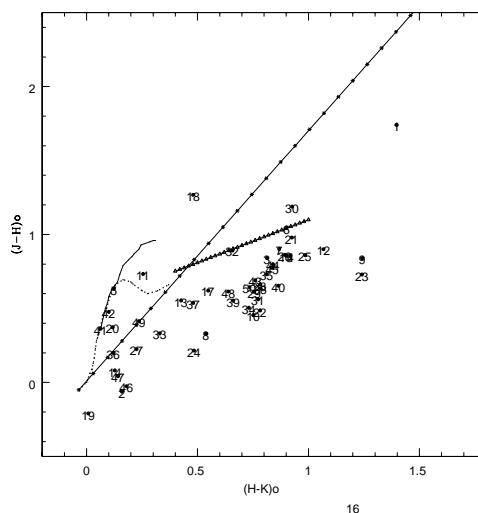
Figure 3. The $(H-K)_0$ vs $(J-H)_0$ reddening corrected colour-colour diagram based on 2MASS data. The location of main-sequence and giants are shown (continuous and dotted curves). The reddening vector, which runs diagonal to the plot is shown with points separated with extinction, A_V of one magnitude. The location of T-Tauri stars are also indicated (line connected by triangular lines). For easy identification, we have shown the identification number of the star in the figure.

HD 250550, CQ Tau, LkH$_\alpha$ 208 and LkH$_\alpha$ 233, V590 Mon, LkH$_\alpha$ 215 and HD 259431 agree with the previous studies of these stars. No previous classification has been done for LkH$_\alpha$ 314, LkH$_\alpha$ 338, MC1, V892 Tau and V1685 Cyg. Hence, we classify these 5 stars as Class I stars, for the first time. The stars having excess in all IR bands are LkH$_\alpha$ 339, V590 Mon, LkH$_\alpha$ 234, LkH$_\alpha$ 215, HD 259431, SV Cep, AS 310. The following objects are found to have difference in classification with respect to previous studies. These are discussed below.

We classify RY Tau to be a Class I star, but in the classification done by Mendigutía et al. (2012) this star is classified under a more evolved stage. Verhoeff et al. (2012) finds that LkH$_\alpha$ 339 has an uncertain evolutionary status with a rising SED with nebulosity in the vicinity. For LkH$_\alpha$ 234, except Fuente et al. (2002) all other studies find that this star is in an earlier evolutionary stage, in agreement with our classification. Mendigutía et al. (2012) grouped SV Cep in a more evolved stage, on the other hand, we find large flux for this star in the 2MASS and WISE pass bands. The previous studies of AS 310 NW support our classification, where it is classified as a less evolved pre-main sequence star with the presence of large flux in mid IR regions, nearby molecular cloud, large grain size and flared disk. Hajjar and Bastien (2000) classified V633 Cas as an extreme Lada Class I star. Maheswar et al. (2002) suggested that it is an early class I star seen through an edge on optically thick disk. According to Fuente et al. (2002) V633 Cas is still immersed in the molecular cloud though not in a dense clump. Similar conclusion was made by Hillenbrand et al. (1992).

Table 2. Table of fluxes in Jansky and respective errors from AKARI (F65, F90, F140, F160) survey.

SI No	Star name	F65	F90	F140	F160	eF65	eF90	eF140	eF160
1	V633 Cas	158.50	122.40	108.80	130.90	6.46	13.90	11.30	23.40
3	AB Aur	97.08	98.55	48.54	76.53	5.80	1.57	6.90	11.80
5	PQ Tau	2.73	4.51	5.80	5.75	0.68	0.47	0.58	0.38
6	RR Tau	1.68	6.99	14.77	20.49	-	0.19	2.04	2.24
7	HD 250550	4.25	6.04	7.96	5.55	0.74	0.53	0.38	0.95
8	LkH$_\alpha$ 208	4.20	7.73	11.11	12.73	0.91	0.55	1.35	0.24
9	LkH$_\alpha$ 338	362.80	607.60	1203.00	2132.00	117.00	-	279.00	756.00
10	LkH$_\alpha$ 339	32.83	32.17	144.40	268.60	9.98	7.67	45.40	24.60
12	V590 Mon	-	32.68	-	-	-	8.70	-	-
13	V360 Mon	171.10	151.20	306.50	441.90	13.20	33.70	69.50	121.00
14	LkH$_\alpha$ 118	21.41	39.43	91.34	123.00	-	2.04	20.80	11.50
15	VV Ser	1.93	3.45	5.80	-	0.37	0.17	1.21	-
16	AS 310 NW	363.90	297.60	400.89	417.50	92.40	56.80	19.20	93.30
17	PX Vul	0.42	0.79	6.63	8.99	-	0.05	0.99	2.90
19	LkH$_\alpha$ 324	72.79	108.80	160.20	196.30	3.94	7.83	17.30	11.60
21	LkH$_\alpha$ 234	932.30	833.70	757.20	880.60	79.40	-	52.70	54.40
22	BD +46^0 3471	1.05	6.04	8.38	15.07	0.63	0.43	2.97	8.34
23	LkH$_\alpha$ 233	23.05	23.17	21.15	23.53	1.11	0.37	5.67	2.86
24	LkH$_\alpha$ 314	9.18	11.92	26.36	24.18	0.87	1.10	6.12	21.00
25	MC1	1.64	3.50	3.22	4.06	0.74	0.24	1.72	1.05
26	VX Cas	0.84	0.74	0.70	0.11	-	0.070	0.11	-
27	RNO 6	30.49	44.45	60.63	65.87	2.61	2.70	5.11	5.020
28	IP Per	5.93	6.39	4.55	2.10	0.19	0.25	0.85	-
29	XY Per EW	3.95	4.36	5.32	1.47	0.52	0.19	0.96	-
30	V892 Tau	57.20	39.04	-	-	1.67	1.64	8.18	-
31	UX Ori	2.73	2.13	4.28	2.23	0.55	0.043	0.60	-
33	P1394	7.47	14.49	53.91	100.30	2.14	2.54	25.00	21.50
34	HD 245185	5.53	4.68	3.79	3.81	0.24	0.23	0.71	-
35	CQ Tau	15.89	16.25	10.30	5.60	1.45	0.37	1.88	0.85
37	BD +26^0 887	4.45	5.00	17.37	14.66	-	0.073	5.42	2.25
39	LkH$_\alpha$ 215	37.44	56.57	128.60	158.00	5.12	1.55	10.90	28.10
40	HD 259431	104.00	111.90	104.80	110.80	13.67	4.77	8.96	8.36
42	W121	6.45	9.82	23.12	20.03	3.41	1.76	13.10	13.00
43	LkH$_\alpha$ 218	2.98	1.22	-	-	0.23	0.11	-	-
44	WW Vul	0.76	1.35	0.36	-	-	0.073	-	-
45	V1685 Cyg	322.50	222.50	255.80	431.90	52.10	60.79	22.70	30.89
46	LkH$_\alpha$ 147	3.25	1.51	5.048	2.17	-	0.26	1.52	-
48	BH Cep	1.15	1.17	1.12	5.77E-02	-	0.055	0.37	1.77
49	BO Cep	1.72	1.568	-	1.69	0.33	0.036	1.65	2.86
50	SV Cep	2.89	1.86	1.55	0.69	0.21	0.069	2.83	0.40

3.2 Class II sources

Class II stars are pre-main sequence stars with optically thick disk. Among the class II stars, the classification for VV Ser, XY Per EW, RR Tau, PX Vul, T Ori, LkH$_\alpha$ 218, UX Ori, WW Vul, V350 Ori, BH Cep and VX Cas agree with most of the previous classification of these stars. No previous classification is done for BD +26^0 887, LkH$_\alpha$ 324, IP Per, P1394 and V360 Mon. Thus these 5 sources are classified as Class II objects for the first time. Sources where we find a different classification are discussed below.

For BD +46^0 3471 and AB Aur, the classification done by Hillenbrand et al. (1992) agree with our classification, but Fuente et al. (2002) proposed the presence of molecular cloud around this star which makes it younger than other Class II stars. In the classification done by Mendigutía et al. (2012) BO Cep is included in a flared, younger, faster evolving disk stage. The studies by Hernandez et al. (2004) conclude that V751 Cyg is a cataclysmic variable with an uncertain evolutionary status. Fuente et al.(2002) grouped RNO 6 under stars which are still immersed in the molecular cloud though not in a dense clump. In the case of HD 245185, Fuente et al. (2002) conclude that it has completely dispersed the surrounding material and are located in a cavity of the molecular cloud but Hillenbrand et al. (1992) grouped this star under disk objects with excess emission above photospheric levels from flat optically thick circumstellar accretion disk. According to Hillenbrand et al. (1992) BD +65^0 1637 comes under emission line stars lacking disk and having small IR excess which is possibly from free-free emission in a gaseous circumstellar disk or envelope but for Fuente et al. (2002) this star has completely dispersed the surrounding material and are located in a cavity of the molecular cloud. In summary, some of our Class II objects are found to be either Class I or Class III sources by other studies. These differences might arise due to the variation in the wavelength coverage of the data, source of the data and the classification scheme.

3.3 Class III sources and sources with TD

Class III stars are diskless pre-main sequence stars which lack infrared excess. These stars are almost at the end stage of its pre-main sequence phase. Previous studies of LkH$_\alpha$ 341, LkH$_\alpha$ 118 also reveal very low excess in IR pass bands of their SED which cause the difficulty in grouping them as main sequence or pre-main sequence objects. LkH$_\alpha$ 118 was rejected by The' et al. (1994) from HAeBe star group. No previous studies have been done for LkH$_\alpha$ 147, BN Ori and LkH$_\alpha$ 201, thus we classify these 3 stars for the first time.

Stars with transition disk, which is a truncated optically thick outer disk with dissipated inner disk, have its characteristic SED with an absence/low level of excess emission from 1.25μm(J)-12μm(W3) micrometer large excess beyond 22μm(W4). Previous studies of PQ Tau is supporting our classification. For V751 Cyg literature gives uncertain evolutionary status (Hernandez et al. (2004)). No previous studies have been done for W121 and VSB2. Hence we classify 2 (3 including V751 Cyg) for the first time.

In summary, the classification based on the WISE colour-colour diagrams shows that most of the classification is in agreement with literature. We have discussed cases where differences have been found. We are able to classify 15 sources for the first time. We revisit this classification based on the spectral energy distribution in the following section.

4.   Classification based on spectral energy distribution

The spectral energy distribution (SEDs) of the pre-main sequence sources is an ideal probe to understand the properties of the source as well as the circumstellar disk. We make us of the multi-wavelength data to construct the SEDs. SEDs are made using an online fitting tool which is available on the website http://caravan.astro.wisc.edu/protostars/sedfitter.php. We follow the YSO SED fitting tool developed by Robitaille et al. (2006, 2007) to estimate the physical properties such as mass, age, accretion rate of disks and envelopes of YSOs. The model compares the observed SEDs using a grid of radiation transfer models for YSOs, which cover a range of stellar masses (0.1 to 50M$_\odot$) and evolutionary stages, so as to compute the mass and age of the central source etc. As mentioned earlier, the extinction and distance for the sources studied here are taken from Table 9 of Hernández et al. (2004). As there is a range in the value of A$_V$, we used a range in extinction (A$_v \sim$ 3-5 mag). The distance used to fit the SED is D ± 100pc, where D corresponds to the distance in Table 9 of Hernández et al. (2004). We have also assumed 10% error in the estimated flux, while fitting the SEDs. The disk and envelope parameters are randomly sampled within the range that depend up on the age of central source. Parameters given by the best fit model are used to characterise the YSOs. The error on these parameters are obtained by finding the deviation of the parameters among the models which fit in the range χ^2 - χ^2_{min} < 3 where χ^2 is the statistical goodness of fit parameter per data point and χ^2_{min} corresponds to the best fit model. Among 50 stars, sources with data in all the 8 pass bands (V,J,H,K,w1,w2,w3,w4) were used to construct SEDs. We used all the pass bands for 33 stars. For 15 stars only infrared magnitudes were used as the visual magnitude is not in agreement with the resulting models. Because of the same reason, W4 magnitude in the case of V633 Cas and, V and J magnitude for V751 Cyg were avoided for fitting SED. From SEDs we can identify each class of stars with their own characteristic appearance (rising/flat/falling). Based on the appearance of the SED, the stars were classified as Class I/II/III and transition disk objects. Initially we derived the SEDs based on the above 8 pass bands. Then we also introduced the AKARI data and derived the SEDs again. As the resolution of the AKARI data is poor, the flux was found to be much larger and the fits were found to be poor. Hence the AKARI flux was used as the upper limit while fitting the SED.

Class I stars have infalling envelope and disk with rising or flat SEDs from 3.3 to 22 μm, while class II stars have falling SED slope starting below from 10 μm which is most probably from an optically thin disk. Class III stars are almost disk less pre-main sequence stars. Stars with transition disk have absence/low level of excess emission from 1-10 μm but large excess beyond 20 μm which might be from a disk with an inner hole. Along with the SEDs, we also derive the parameters of the central source as well as the circumstellar disk. Tables 4, 6, 8 and 10 list out the stellar parameters of Class I, II, III and Transition disk objects respectively.
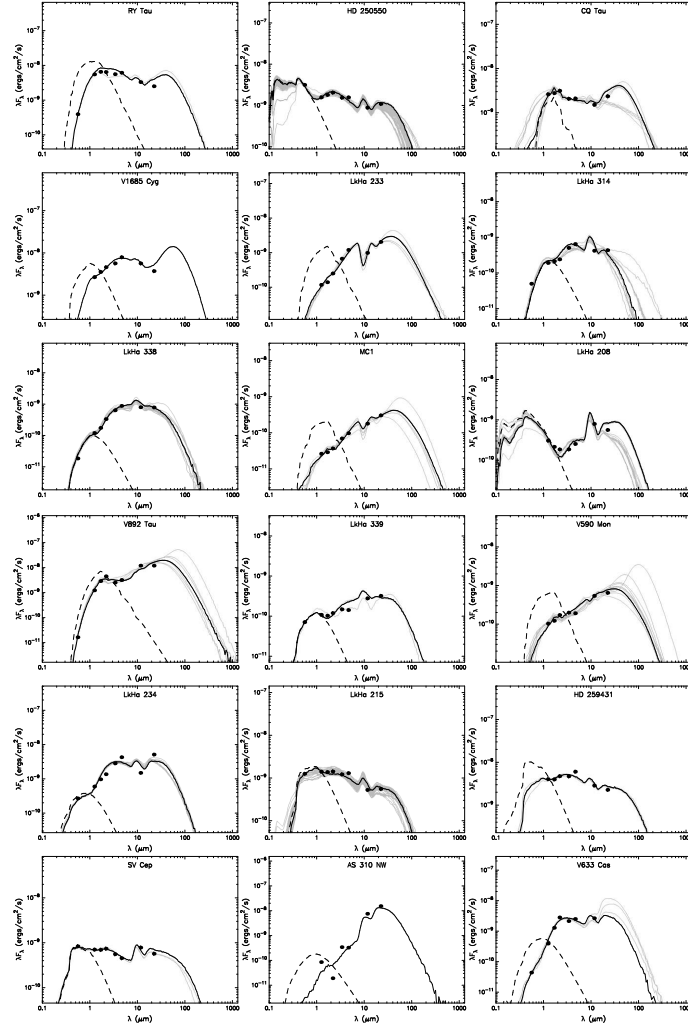
Figure 4. The SEDs and fit to the SEDs of Class I stars(RY Tau, HD 250550, CQ Tau, V1685 Cyg, LkH$_\alpha$ 233, LkH$_\alpha$ 314, LkH$_\alpha$ 338, MC1, LkH$_\alpha$ 208, V892 Tau, LkH$_\alpha$ 339, V590 Mon, LkH$_\alpha$ 234, LkH$_\alpha$ 215, HD 259431, SV Cep, AS 310 NW, V633 Cas respectively). The filled circles show the input fluxes. The black line shows the best fit, and the gray lines show subsequent good fits. The dashed line shows the stellar photosphere corresponding to the central source of the best fitting model, as it would look in the absence of circumstellar dust (but including interstellar extinction). The grey lines represent models which are within the χ^2_{min} - χ^2_{best} < 3 limit.
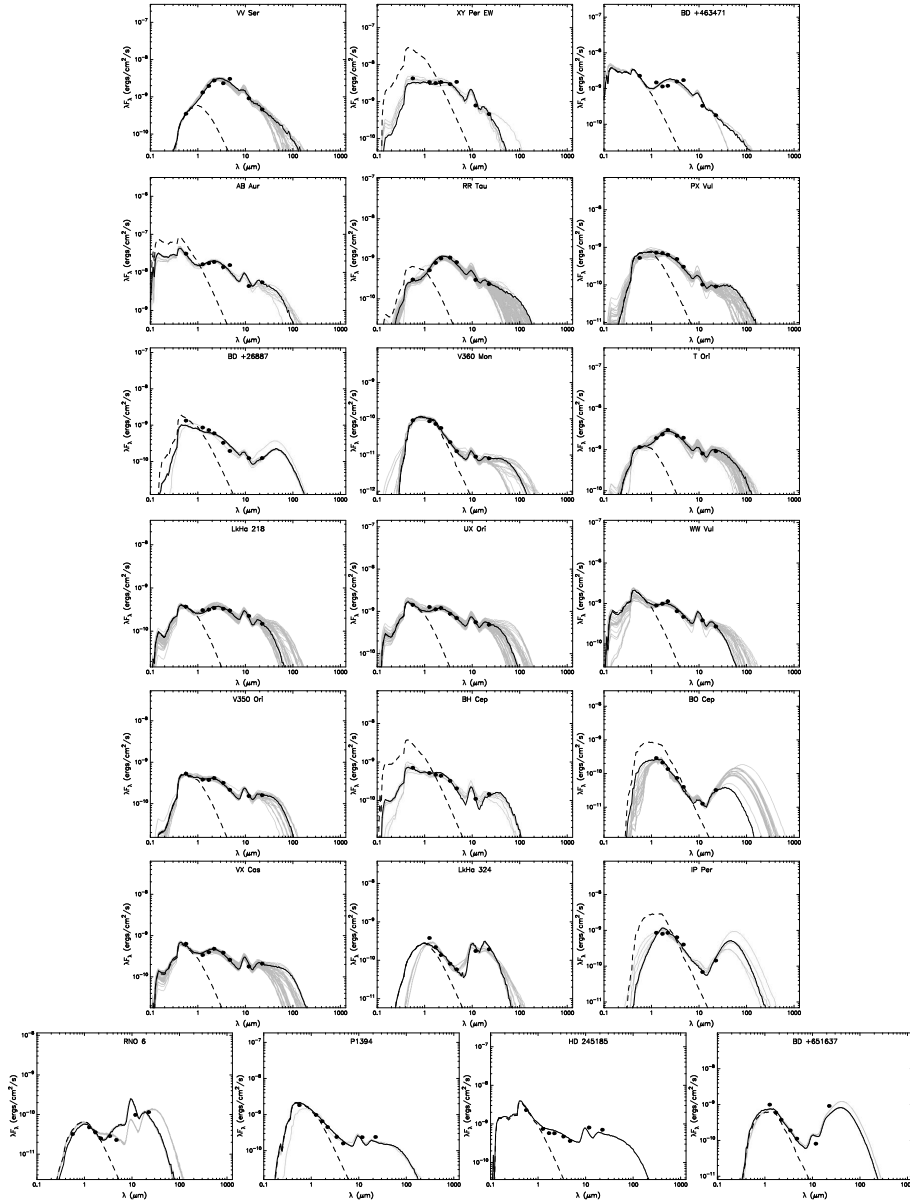
Figure 5. The SEDs and fit to the SEDs of Class II stars (VV Ser, XY Per EW, BD +46^0 3471, AB Aur, RR Tau, PX Vul, BD +26^0 887, V360 Mon, T Ori, LkH$_\alpha$ 218, UX Ori, WW Vul, V350 Ori, BH Cep, BO Cep, VX Cas, V751 Cyg, LkH$_\alpha$ 324, IP Per, RNO 6, P1394, HD 245185, BD +65^0 1637 respectively). The filled circles show the input fluxes. The black line shows the best fit, and the gray lines show subsequent good fits. The dashed line shows the stellar photosphere corresponding to the central source of the best fitting model, as it would look in the absence of circumstellar dust (but including interstellar extinction).
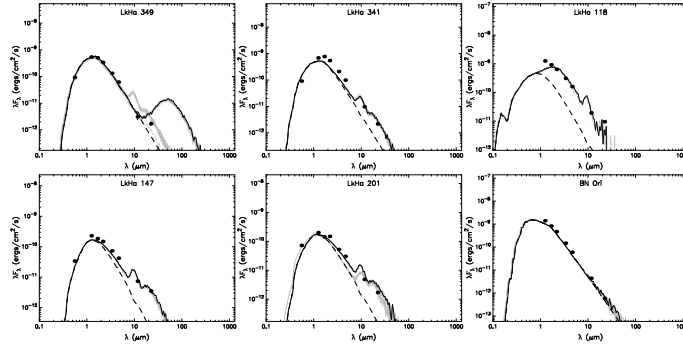
Figure 6. The SEDs and fit to the SEDs of Class III stars (LkH$_\alpha$ 349, LkH$_\alpha$ 341, LkH$_\alpha$ 118, LkH$_\alpha$ 147, LkH$_\alpha$ 201BN Ori respectively). The filled circles show the input fluxes. The black line shows the best fit, and the gray lines show subsequent good fits. The dashed line shows the stellar photosphere corresponding to the central source of the best fitting model, as it would look in the absence of circumstellar dust (but including interstellar extinction).

4.1 Class I sources

The shape of SEDs of Class I stars more or less agree with the classifications based on the WISE colour-colour diagram. The SEDs of 18 Class I sources are shown in Fig. 4. SEDs of LkH$_\alpha$ 339, V590 Mon, LkH$_\alpha$ 234, LkH$_\alpha$ 215, HD 259431, V633 Cas, SV Cep show large IR excess. Age is a parameter derived from the SED fits, which can be used to check the classification. Our study derives much lower age range for RY Tau, CQ Tau, MC1, LkH$_\alpha$ 208, V892 Tau, LkH$_\alpha$ 233, than given in the literature. The derived parameters for V590 Mon, LkH$_\alpha$ 234, LkH$_\alpha$ 215 supports our classification. The derived ages for LkH$_\alpha$ 339, HD 259431,SV Cep are much larger. Previous studies of LkH$_\alpha$ 234, LkH$_\alpha$ 215,HD 25943 find that they are younger stars while LkH$_\alpha$ 339, V590 Mon, SV Cep, HD 250550, LkH$_\alpha$ 314, LkH$_\alpha$ 338 and V1685 Cyg are much older than typical Class I stars.

4.2 Class II sources

The SEDs of 22 Class II sources are shown in Fig. 5. Previous studies of PX Vul suggested that it is in a highly evolved stage but SED derived here estimates younger age. SEDs of BO Cep, LkH$_\alpha$ 324, IP Per and BD +65^0 1637 suggest that their disk might evolve to become transition disks. The derived ages for V360 Mon, UX Ori, V350 Ori, VX Cas are much higher than that of typical Class II stars. Hernandez et al. (2004) derived an older age (12.5Myr) for V360 Mon, and for others literature gives younger ages than our estimate. The derived ages of these stars ranges from 0.3 Myr to 2.3 Myr. Previous studies also gives this distributed behaviour in age for Class II sources, which ranges from 0.001 Myr to 14.36 Myr.
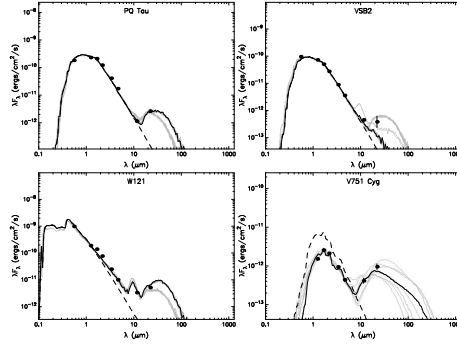
Figure 7. The SEDs and fit to the SEDs of Stars with transition disk (PQ Tau, VSB2, W121, V751 Cyg respectively). The filled circles show the input fluxes. The black line shows the best fit, and the gray lines show subsequent good fits. The dashed line shows the stellar photosphere corresponding to the central source of the best fitting model, as it would look in the absence of circumstellar dust (but including interstellar extinction).

4.3 Class III sources and sources with TD

The SEDs of 6 Class III sources are shown in Fig. 6. Even though SEDs of Class III stars support this conclusion, age derived from SEDs show very young ages. There is no previous estimation of age for LkH$_\alpha$ 147 and LkH$_\alpha$ 201. Hernandez et al. (2004) estimated the age of LkH$_\alpha$ 341 as 7.90Myr and previous studies of other stars found that they are younger Class III stars.

SEDs and derived age ranges of PQ Tau, VSB2, V751 Cyg and W121 support our classification as stars having transition disk. The SEDs of 4 transition disk sources are shown in Fig. 7. Hernandez et al. (2004) estimated an age of 11.74 Myr for VSB2. Derived ages of transition disk sources range between 2-7 Myr.

4.4 SEDs including AKARI data

The AKARI data are found to be available for 40 sources. The data is tabulated in Table 2. We have derived the SEDs for sources after including the AKARI data. As we used the AKARI fluxes as upper limits while deriving the SEDs, the data points are shown as triangles in the SEDs. The SEDs for the Class I, II, III and TDs are shown in Figs 8, 9, 10 and 11 respectively. If we compare the SEDs derived with and without the AKARI data, we notice that even though many SEDs look similar, a number of SEDs show mildly better fits based on the χ^2 value. We obtained relatively better fits for CQ Tau, HD 250550, LKH$_\alpha$ 233, V892 Tau, V 590 Mon, SV Cep, AB Aur, LKH$_\alpha$ 218, UX Ori, WW Vul, BH Cep, VX Cas, IP Per, HD 245185. The SED fits are found not to change significantly with the inclusion of AKARI data for most of the sources, but the χ^2 value, the error of the estimated parameters as well as the number of models used to fit the data were
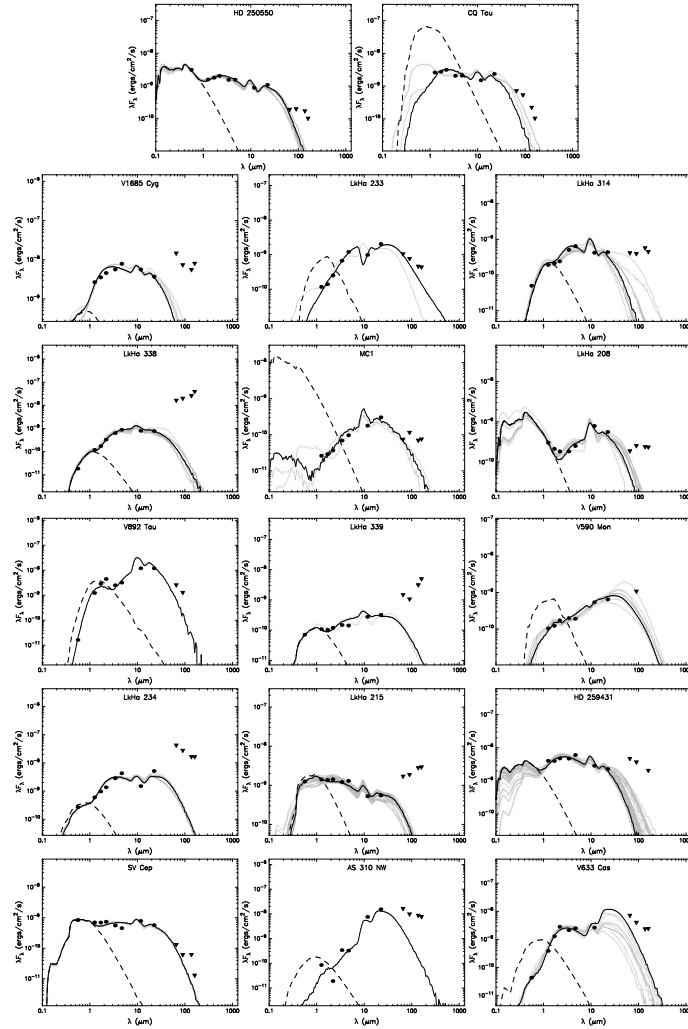
Figure 8. The SEDs plotted using 2MASS, WISE and AKARI data of Class I stars (HD 250550, CQ Tau, V1685 Cyg, LkH$_\alpha$ 233, LkH$_\alpha$ 314, LkH$_\alpha$ 338, MC1, LkH$_\alpha$ 208, V892 Tau, LkH$_\alpha$ 339, V590 Mon, LkH$_\alpha$ 234, LkH$_\alpha$ 215, HD 259431, SV Cep, AS 310 NW, V633 Cas respectively). The filled circles show the input fluxes. The black line shows the best fit, and the gray lines show subsequent good fits. The dashed line shows the stellar photosphere corresponding to the central source of the best fitting model, as it would look in the absence of circumstellar dust (but including interstellar extinction).
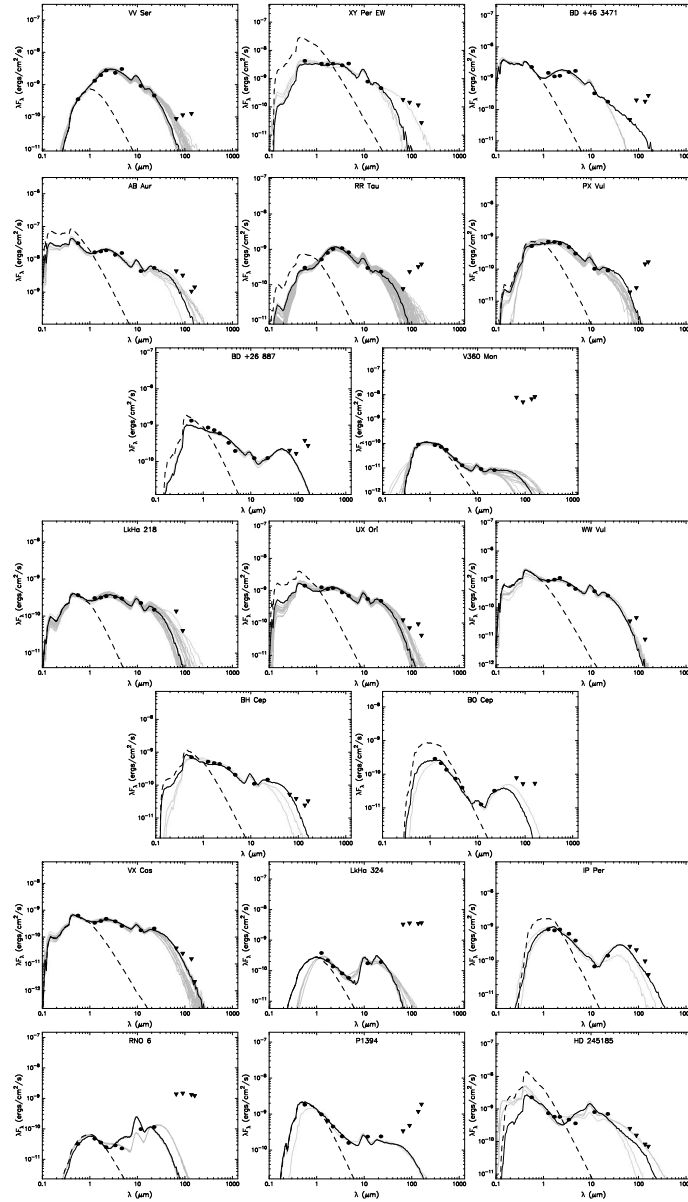
Figure 9. The SEDs plotted using 2MASS, WISE and AKARI data of Class II stars (VV Ser, XY Per EW, BD +46^0 3471, AB Aur, RR Tau, PX Vul, BD +26^0 887, V360 Mon, LkH$_\alpha$ 218, UX Ori, WW Vul, BH Cep, BO Cep, VX Cas, LkH$_\alpha$ 324, IP Per, RNO 6, P1394, HD 245185 respectively). The filled circles show the input fluxes. The black line shows the best fit, and the gray lines show subsequent good fits. The dashed line shows the stellar photosphere corresponding to the central source of the best fitting model, as it would look in the absence of circumstellar dust (but including interstellar extinction).
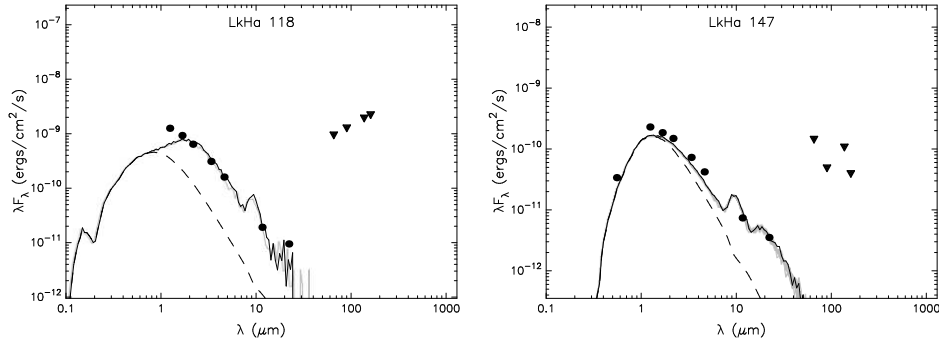
Figure 10. The SEDs plotted using 2MASS, WISE and AKARI data of Class III stars (LkH$_\alpha$ 118, LkH$_\alpha$ 147 respectively). The filled circles show the input fluxes. The black line shows the best fit, and the gray lines show subsequent good fits. The dashed line shows the stellar photosphere corresponding to the central source of the best fitting model, as it would look in the absence of circumstellar dust (but including interstellar extinction).

Figure 11. The SEDs plotted using 2MASS, WISE and AKARI data of Stars with transition disk (PQ Tau, W121 respectively). The filled circles show the input fluxes. The black line shows the best fit, and the gray lines show subsequent good fits. The dashed line shows the stellar photosphere corresponding to the central source of the best fitting model, as it would look in the absence of circumstellar dust (but including interstellar extinction).
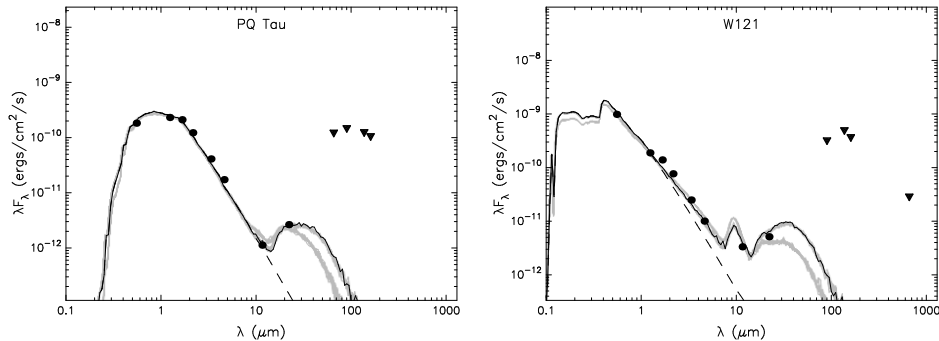
found to improve, except in the case of HD 250550 and MC1. Thus, we find that, for a good fraction of HAeBe stars, we do not detect a marked improvement in the derived parameters due to the inclusion of AKARI data. We suspect that, due to the large PSF of the AKARI data, the flux obtained in the longer wavelengths come from the material in the vicinity of the source and much beyond its disk. We also suspect that the flux may also include contributions from nearby sources, especially in dense regions. Hence in many cases, the AKARI flux is much more than what is expected. The SEDs including AKARI data are not used for classification, but we use the derived parameters in the next section.

Table 3. Summary of classification of HAeBe stars based on two methods compared with the results from the literature. The method 1 is the classification based on WISE colours and method 2 is the classification based on SEDs. TD corresponds to transition disk objects.

SI No	Star name	Class based on method 1 (CCD)	Class based on method 2 (SED)	literature class
1	V633 Cas	–	Class I	Class I
2	LkH$_\alpha$ 201	Class III	Class III	no previous classification
3	AB Aur	Class II	Class II	Class II
4	T Ori	Class II	Class I	Class II
5	PQ Tau	T D	T D	no previous classification
6	RR Tau	Class II	Class I	Class II
7	HD 250550	Class I	Class I	Transition from Class I to Class II
8	LkH$_\alpha$ 208	Class I	Class I	Class II
9	LkH$_\alpha$ 338	Class I	Class I	no previous classification
10	LkH$_\alpha$ 339	–	Class I	no previous classification
11	LkH$_\alpha$ 341	Class III	Class III	Class III
12	V590 Mon	–	Class I	Class I
13	V360 Mon	Class II	Class II	no previous classification
14	LkH$_\alpha$ 118	Class III	Class III	Class III
15	VV Ser	Class II	Class I	Class II
16	AS 310 NW	–	Class I	Class I
17	PX Vul	Class II	Class II	Class II
18	V751 Cyg	T D	T D	no previous classification
19	LkH$_\alpha$ 324	–	Class II	no previous classification
20	LkH$_\alpha$ 349	Class III	Class III	no previous classification
21	LkH$_\alpha$ 234	–	Class I	Class I
22	BD +46^0 3471	Class II	Class II	Class II
23	LkH$_\alpha$ 233	Class I	Class I	Transition from Class I to Class II
24	LkH$_\alpha$ 314	Class I	Class I	no previous classification
25	MC1	Class I	Class I	no previous classification
26	VX Cas	Class II	Class II	Class II
27	RNO 6	–	Class II	Class II
28	IP Per	–	Class II	no previous classification
29	XY Per EW	Class II	Class II	Class II
30	V892 Tau	Class I	Class I	no previous classification
31	UX Ori	Class II	Class II	Class II
32	RY Tau	Class I	Class I	Class II
33	P1394	–	Class II	no previous classification
34	HD 245185	–	Class II	Transition from Class II to Class III
35	CQ Tau	Class I	Class I	Class I
36	BN Ori	Class III	Class III	no previous classification
37	BD +26^0 887	Class II	Class II	no previous classification
38	V350 Ori	Class II	Class II	Class II

Table 3. Continued.

SI No	Star name	Class based on method 1 (CCD)	Class based on method 2 (SED)	literature class
39	LkH$_\alpha$ 215	–	Class I	Class II
40	HD 259431	–	Class I	Transition from Class I to Class II
41	VSB2	T D	T D	no previous classification
42	W121	T D	T D	no previous classification
43	LkH$_\alpha$ 218	Class II	Class II	Class III
44	WW Vul	Class II	Class II	Class II
45	V1685 Cyg	Class I	Class I	Class II
46	LkH$_\alpha$ 147	Class III	Class III	no previous classification
47	BD +65^0 1637	Class II	Class II	Class III
48	BH Cep	Class II	Class II	Class II
49	BO Cep	Class II	Class II	T D
50	SV Cep	–	Class I	Class II

Table 4. Table of derived star parameters of Class I stars from SED fits (A - Age of star in Myr, eA – Error in age of star, M - Mass of star in M$_\odot$, eM – Error in mass of star, RR – Sublimation Radius of the star in AU, eRR – Error in sublimation radius, RA – Inner radius of the star in AU, eRA – Error in inner radius of the star, T – Temperature of the star in Kelvin, eT – Error in temperature of the star.)

STAR	A	eA	M	eM	RR	eRR	RA	eRA	T	eT
RY Tau	0.24	0.24	6.43	0.19	1.00	0.52	1.63	0.65	7462	2425
HD 250550	2.05	0.26	4.38	0.04	1.00	0.03	1.30	0.06	15220	114
CQ Tau	0.04	0.43	0.31	0.36	1.00	1.13	0.15	0.33	3387	429
LkH$_\alpha$ 314	3.20	0.28	2.99	0.09	8.05	0.33	4.79	0.64	10720	338
LkH$_\alpha$ 338	5.35	0.54	4.50	0.07	6.92	0.20	9.45	0.48	15430	216
MC1	0.008	0.002	0.72	0.14	1.00	1.17	0.23	0.59	3858	53
LkH$_\alpha$208	1.24	0.29	4.61	0.20	18.54	0.99	28.06	1.90	15520	657
V892 Tau	0.008	0.005	1.01	0.11	1.00	0.96	0.33	0.31	3967	37
V1685 Cyg	3.22	0.25	7.46	0.08	1.00	0.09	3.63	0.45	21460	163
LkH$_\alpha$ 23	0.004	0.12	1.89	0.56	1.11	1.37	0.77	2.88	4162	1655
AS 310 NW	2.97	0.57	10.92	0.77	9.16	2.03	66.69	14.05	26900	827
V633 Cas	0.68	0.45	6.15	0.17	1.00	0.34	2.49	0.65	18860	626
LkH$_\alpha$ 339	7.99	0.72	3.27	0.07	11.15	0.69	8.25	0.85	12570	162
V590 Mon	0.007	0.003	2.00	0.23	1.00	0.67	0.55	0.22	4167	56
LkH$_\alpha$ 234	0.78	0.46	6.86	0.04	3.48	0.18	10.62	0.58	20280	76
LkH$_\alpha$ 215	0.82	0.03	4.50	0.03	1.99	0.11	2.44	0.11	9147	296
HD 259431	3.19	0.17	6.25	0.05	1.00	0.04	2.53	0.11	19000	146
SV Cep	8.3	0.9	2.57	0.06	1.00	0.56	0.48	0.32	10730	83

The results of the classification using the above two methods are summarised in Table 3. We adopt the final classification from the SEDs. We could successfully classify 50 sources into 4 groups (Class I, II, III and Transition disk objects), of which 18 are classified for the first time. We classified 18 sources as Class I (5 classified for the first time), 22 sources as Class II

Annapurni Subramaniam and B. Adara

Table 5. Table of derived disk parameters of Class I stars from SED fits (DM – disk mass ($M_{\odot}$) in log scale in , eDM – error in disk mass, DA – disk accretion rate ($M_{\odot}$/year) in log scale, eDA – error in disk accretion rate, χ^2 – per number of data points of best fit model, N – Number of models used to estimate the average and error of parameters.

STAR	DM	eDM	DA	eDA	χ^2	N
RY Tau	-1.55	-2.04	-6.75	-6.94	10.4	10
HD 250550	-2.89	-2.50	-9.15	-7.56	1.2	95
CQ Tau	-1.62	-2.22	-5.71	-6.41	3.4	19
LkH$_\alpha$ 314	-2.40	-2.89	-9.08	-8.82	12.9	47
LkH$_\alpha$ 338	-1.92	-2.83	-7.70	-8.62	2.4	26
MC1	-2.09	-2.05	-7.66	-5.91	3.3	13
LkH$_\alpha$ 208	-5.34	-2.86	-9.73	-7.50	6.8	42
V892 Tau	-2.90	-2.23	-8.31	-6.51	6.6	21
V1685 Cyg	-2.52	-1.99	-7.76	-6.56	6.7	30
LkH$_\alpha$ 23	-0.82	-1.65	-4.80	-5.44	4.5	16
AS 310 NW	-6.07	-0.84	-12.25	-5.61	68.5	9
V633 Cas	-1.00	-0.40	-7.08	-7.12	5.1	23
LkH$_\alpha$ 339	-3.72	-1.07	-8.28	-9.08	7.2	14
V590 Mon	-1.48	-1.08	-5.98	-6.30	4.0	19
LkH$_\alpha$ 234	-2.09	-2.33	-8.01	-8.29	12.9	21
LkH$_\alpha$ 215	-3.98	-2.60	-9.10	-7.99	2.7	84
HD 259431	-3.40	-2.75	-9.32	-7.32	4.2	98
SV Cep	-1.35	-2.01	-7.13	-7.76	4.4	9

(5 classified for the first time), 6 sources as Class III (4 classified for the first time) and 4 sources with Transitional Disk (all four sources are classified for the first time). Thus, we have achieved classification of about one third of the sample for the first time. We would like to point out that the results derived here more or less agree with the those in the literature for sources with previous studies. We do see an overlap between Class I and Class II sources and similarly with Class II and Class III sources. These could be due to the limited pass bands used here and also because of the degeneracy arising in the derived SEDs. Hence better classification and clarity will emerge with the addition of better FIR data.

5. Estimation of star and disk parameters

We have derived various parameters of the central source and the circumstellar disk using the SEDs. The derived parameters are: Age of star in million years, error in age, mass of star in $M_{\odot}$, error in mass, sublimation radius of the star in AU, error in sublimation radius, inner radius of the star in AU, error in inner radius, temperature of the star in Kelvin, error in temperature, disk mass (in log) in $M_{\odot}$, error in disk mass, disk accretion rate of the star (in log) of mass in $M_{\odot}$ /year, error in disk accretion rate, χ^2 per number of data points of best fit model and number of models used to estimate the average and errors of the above parameters. The above parameters derived

Table 6. Table of derived star parameters of Class II stars from SED fits. The parameters are same as Table 4.

STAR	A	eA	M	eM	RR	eRR	RA	eRA	T	eT
VV Ser	1.52	0.23	3.89	0.05	1.00	0.03	1.13	0.04	12940	214
XY Per EW	3.01	1.57	3.23	0.30	1.00	0.29	0.77	0.08	12330	815
BD +46^0 3471	1.64	0.44	4.84	0.05	1.00	0.01	1.57	0.03	16200	96
AB Aur	3.69	0.49	4.16	0.11	1.00	0.03	1.17	0.05	14670	286
RR Tau	4.61	0.13	4.39	0.02	1.49	0.03	1.93	0.04	15190	66
PX Vul	4.58	0.19	2.51	0.04	1.00	0.02	0.43	0.02	9480	222
BD +26^0 887	0.43	0.22	5.49	0.28	1.00	0.01	1.53	0.28	8646	1677
V360 Mon	7.02	0.55	1.77	0.04	1.49	0.48	0.23	0.10	5590	83
T Ori	1.76	0.24	4.74	0.06	1.00	0.01	1.50	0.03	15980	183
LkH$_\alpha$ 218	2.74	0.27	3.32	0.07	1.00	0.06	0.91	0.09	12250	195
UX Ori	6.99	0.23	3.14	0.03	1.00	0.02	0.68	0.02	12250	97
WW Vul	3.16	0.36	2.85	0.06	1.00	0.04	0.67	0.03	10620	233
V350 Ori	7.20	0.27	2.37	0.04	1.00	0.13	0.40	0.08	10130	128
BH Cep	4.27	0.44	2.43	0.06	1.00	0.05	0.47	0.05	8459	361
BO Cep	0.57	0.03	0.79	0.05	1.00	0.07	0.11	0.01	4106	56
VX Cas	10.0	0.5	3.42	0.04	1.00	0.02	0.80	0.02	12930	109
LkH$_\alpha$ 324	2.24	0.14	5.36	0.37	1.00	4.29	1.90	1.95	17230	2021
IP Per	0.36	0.03	3.95	0.48	1.00	0.14	0.41	0.04	4867	116
RNO 6	3.32	0.22	5.14	0.08	20.82	1.73	36.30	3.25	16750	202
RY Tau	2.88	0.32	2.68	0.05	7.02	1.05	2.81	0.55	6354	273
HD 245185	4.89	0.45	2.80	0.14	1.00	1.92	0.57	1.20	11390	387
BD +65^0 1637	0.26	0.03	5.26	0.34	1.00	0.10	0.81	0.06	5136	125

without AKARI data, are given in Tables 4 and 5 for Class I sources, Tables 6 and 7 for Class II sources, Tables 8 and 9 for Class III sources and Tables 10 and 11 for transition disk sources.

5.1 Class I sources

It can be seen that the χ^2 values take a range for the Class I sources and the best fit is obtained for HD250550, with a χ^2 fit of 1.2 using 95 models. AS310 NW has the poorest SED fit, as this source is found to be an outlier in most of the plots.

Nine Class I sources are found to be younger than 1 Myr, as expected for Class I sources. On the other hand, 9 sources are older than 1 Myr with SV Cep and LKH$_\alpha$ 339 with $\sim$ 8 Myr. The masses are found to be from sub-solar to $\sim$ 10 M$_\odot$. The inner radius as well as the sublimation radius are found to be a function of the temperature. Among the Class I sources, V633 Cas (0.7 Myr) is found to have the largest disk mass ($\sim$ 0.1 M$_\odot$) and LKH$_\alpha$ 23 (0.1M$_\odot$ /year) has the maximum disk accretion rate. CQ Tau and MC1 are found to be sub-solar mass sources, which are very young relatively cool (T $\leq$ 4000 K) sources. These sources have disk mass $\sim$ 0.001 - 0.01 M$_\odot$ and relatively large disk accretion. The derived parameters for AS310 are also found to be a

Table 7. Table of derived disk parameters of Class II stars from SED fits. The parameters are same as Table 5.

STAR	DM	eDM	DA	eDA	χ^2	N
VV Ser	-4.74	-2.46	-9.28	-7.58	2.3	88
XY Per EW	-6.65	-2.73	-10.86	-9.41	6.9	11
BD +46^0 3471	-5.03	-3.14	-9.69	-8.10	8.7	61
AB Aur	-1.85	-2.52	-8.45	-7.49	4.3	50
RR Tau	-3.21	-2.72	-8.04	-7.71	1.2	305
PX Vul	-1.62	-2.93	-8.30	-7.70	1.9	90
BD +26^0 887	-2.47	-1.70	-7.94	-7.38	6.1	21
V360 Mon	-5.02	-2.83	-11.48	-8.38	1.6	55
T Ori	-3.97	-2.62	-8.79	-7.71	1.1	129
LkH$_\alpha$ 218	-1.26	-2.68	-6.00	-7.06	1.5	122
UX Ori	-2.24	-2.72	-8.75	-8.31	1.4	97
WW Vul	-3.86	-2.92	-8.82	-8.44	1.7	89
V350 Ori.	-3.10	-3.39	-9.28	-9.43	0.6	49
BH Cep	-3.36	-3.28	-8.85	-8.37	2.7	29
BO Cep	-4.80	-3.21	-10.70	-8.81	3.0	122
VX Cas	-2.82	-2.77	-9.15	-8.29	0.9	95
LkH$_\alpha$ 324	-7.16	-2.60	-13.95	-9.20	3.5	23
IP Per	-2.99	-2.20	-8.67	-7.73	6.1	22
RNO 6	-5.47	-3.20	-11.34	-9.69	10.3	32
RY Tau	-1.33	-2.21	-6.97	-7.18	7.3	43
HD 245185	-1.96	-2.21	-7.28	-7.90	13.1	18
BD +65^0 1637	-2.13	-2.18	-7.77	-7.56	13.7	18

Table 8. Table of derived star parameters of Class III stars from SED fits. The parameters are same as Table 4.

STAR	A	eA	M	eM	RR	eRR	RA	eRA	T	eT
LkH$_\alpha$ 349	1.27	0.03	3.46	0.02	1.00	8.37	0.47	3.63	5752	37
LkH$_\alpha$ 341	1.27	0.02	3.46	0.01	1.00	0.01	0.47	0.01	5752	18
LkH$_\alpha$ 118	1.30	0.00	14.60	0.00	1.00	0.00	11.27	0.00	30960	0
LkH$_\alpha$ 147	3.14	0.00	2.71	0.00	1.00	0.00	0.520	0.00	7971	0
LkH$_\alpha$ 201	3.14	0.12	2.71	0.07	1.00	16.75	0.52	12.96	7971	392
BN Ori	2.688	0.00	2.53	0.00	312.90	0.00	79.17	0.00	5507	0

different. We find this star to be a very massive ~ 10 M$_\odot$, hot (~ 27000 K) star of about 3 Myr age, but still in the Class I evolutionary stage. The AKARI data confirms the expected large flux at longer wavelengths. The source has the least disk accretion and lowest disk mass among the Class I sources. Hence, the source is likely to be embedded in a cloud hence it shows relatively large excess at longer wavelengths.

Table 9. Table of derived disk parameters of Class III stars from SED fits. The paramaters are same as Table 5.

STAR	DM	eDM	DA	eDA	χ^2	N
LkH$_\alpha$ 349	-6.87	-2.29	-13.77	-12.93	5.0	35
LkH$_\alpha$ 341	-6.87	-1.66	-13.77	-12.90	23.8	15
LkH$_\alpha$ 118	-8.04	-1.23	-9.44	-17.63	30.2	2
LkH$_\alpha$ 147	-7.10	-2.97	-12.92	-20.99	9.3	5
LkH$_\alpha$ 201	-7.10	-3.78	-12.92	-12.58	15.4	15
BN Ori	-7.62	-2.61	-13.02	-21.80	6.8	6

Table 10. Table of derived star parameters of stars with transition disk, from SED fits. The parameters are same as in Table 4.

STAR	A	eA	M	eM	RR	eRR	RA	eRA	T	eT
PQ Tau	6.3	0.8	1.78	0.04	323.0	28.2	43.6	4.0	5369	101
VSB2	5.06	0.29	1.96	0.03	50.1	37.3	8.3	5.4	5453	29
W121	6.2	0.2	2.64	0.03	1.00	0.00	0.49	0.01	10920	87
V751 Cyg	1.9	0.5	0.56	0.10	57.1	12.9	2.7	1.1	3843	148

5.2 Class II sources

In the case of Class II sources, the age is estimated to be between 1-7 Myr and the mass is found to be between 2-6 M$_\odot$. 4 sources are found to be younger than 1 Myr and 2 sources have mass less than 2 M$_\odot$. None of the Class II sources are found to be massive than $\sim$ 6 M$_\odot$, in contrast to 6 more massive sources among the Class I. This might indicate that sources more massive than $\sim$ 6 M$_\odot$ have a very short Class II phase such that they are not detected in this phase. As expected, the Class II sources have relatively less mass in the disk and low accretion rates. LKH$_\alpha$ 218 has the maximum disk mass (0.05 M$_\odot$) and largest accretion rate.

5.3 Class III sources and sources with TDs

The Class III sources are found to be between 1-3 Myr old with mass in the 2-3 M$_\odot$ range, except for one star LKH$_\alpha$ 118 where only two models is found to fit the data (hence the result may be

Table 11. Table of derived disk parameters of stars with transition disk, from SED fits. The parameters are same as in Table 5.

STAR	DM	eDM	DA	eDA	χ^2	N
PQ Tau	-5.60	-2.67	-12.44	-13.05	2.4	21
VSB2	-7.68	-3.51	-12.62	-13.61	3.6	44
W121	-7.23	-4.18	-13.70	-13.20	4.8	22
V751 Cyg	-4.60	-1.89	-10.38	-9.08	2.5	20

unreliable). These sources have very poor disks and almost nil disk accretion. The χ^2 fit for the SEDs are in general poor and the number of models which fall within the specified χ^2 range with respect to the the best fitting model is also small. In a few cases, the stellar parameters of all the models averaged within the χ^2 limit are the same, such that error in the parameters could not be estimated. On the other hand, we do estimate substantial errors for their disk parameters. Three of the 4 transition disk sources are found to be older than 5 Myr and have mass around 2 $M_\odot$. For these four sources good χ^2 values are obtained for the SED fits, with ≥ 20 models used to obtain the errors in the estimated parameters resulting in relatively less errors. Thus, we identify and reliably estimate the parameters of 4 sources with transition disk in this study.

The parameters estimated here are using the SED fitting technique using data of up to 8 pass bands. The estimated parameters could be biased due to the degeneracy in the derived star/disk parameters. We have tried to increase the reliability of the derived parameters by including the AKARI data. The AKARI data is used as upper limit and the parameters derived after including the AKARI data are tabulated in Tables 12 and 13. It can be seen that the χ^2 fit for some sources are slightly better resulting in mild reduction of errors, while the estimated parameters more or less remain the same. We also notice an increase in the number of models which are present within the considered χ^2 range. We notice that by including the AKARI data, the age of AB Aur is found to increase from 3.7 to 7.6 Myr. The source AS 310 MW is found to be more massive and younger, whereas the source MC1 is found to be more massive and older. As there is a variation in the derived parameters with and without AKARI data (as an upper limit), we have tabulated the estimated parameters with and without AKARI data.

When we compare the parameters estimated with and without AKARI data, we notice variations. Hence for the comparative study, presented in the next section, we adopt the following. The SED fit parameters are taken including the AKARI data for sources with better fits (38 sources) and parameters without AKARI data are taken for 12 sources.

6.   Discussion

This study has classified 50 HAeBe sources in to 4 groups and estimated their stellar disk parameters. The high light of the study is the analysis of large number of stars, but the draw back is the absence of reliable FIR data. We try to understand the variation in parameters as a function of mass and age of all the sources together. For a comparative study, we have taken disk parameters 50 sources, where the parameters are derived including AKARI data for 38 sources and without AKARI data for 12 sources. Fig. 12 shows the relation between the derived mass and age of the stars. Stars belonging to various classes are shown separately using different symbols and the estimated errors are also shown. The Class I sources are the relatively younger and many of them are also massive. The Class II sources have a range in mass, with an upper limit of mass in the range of ~ 6 $M_\odot$. The upper limit is only indicative in this study and a larger sample is needed to confirm this suggestion. The sample studied here have mass in the range 2-8 $M_\odot$ (except for 6 sources) and age in the range 0.1 - 8 Myr.

Table 12. SED derived parameters using WISE,2MASS,AKARI data. The parameters are same as in Table 4.

N0	STAR	A	EA	M	EM	RR	ERR	RA	ERA	T	ET
1	V633 Cas	0.68	0.34	6.15	0.17	1.00	0.31	2.49	0.62	18860	506
3	AB Aur	7.62	0.27	3.36	0.02	1.00	0.02	0.79	0.02	12780	64
5	PQ Tau	6.289	0.579	1.78	0.03	323.000	18.109	43.640	2.445	5369.0	75
6	RR Tau	4.614	0.117	4.39	0.02	1.487	0.030	1.933	0.039	15190.0	64
7	HD 250550	2.051	0.307	4.38	0.07	1.000	0.018	1.299	0.049	15220.0	137
8	LkH$_\alpha$ 208	1.087	0.286	4.51	0.18	14.640	0.620	20.510	1.768	14130.0	476
9	LkH$_\alpha$ 338	5.350	0.342	4.50	0.05	6.922	0.204	9.453	0.459	15430.0	126
10	LkH$_\alpha$ 339	5.285	0.415	3.36	0.12	7.695	0.887	6.003	1.579	12800.0	286
12	V590 Mon	0.015	0.004	1.33	0.09	1.000	0.562	0.392	0.208	4117.0	37
13	V360 Mon	7.018	0.405	1.77	0.03	1.488	0.629	0.234	0.118	5593.0	62
14	LkH$_\alpha$ 118	1.30	0.00	14.60	0.00	1.00	0.00	11.27	0.00	30960	0
15	VV Ser	1.52	0.25	3.89	0.06	1.00	0.02	1.13	0.04	12940	228
16	AS 310 NW	0.77	0.42	13.09	0.50	1.00	1.53	9.64	10.70	29430	563
17	PX Vul	3.90	0.22	2.58	0.04	1.00	0.02	0.56	0.03	9722	193
19	LkH$_\alpha$ 324	2.24	0.10	5.36	0.30	1.00	4.01	1.90	2.17	17230	1573
21	LkH$_\alpha$ 234	4.47	0.62	7.18	0.07	3.67	0.22	12.29	0.61	20880	167
22	BD +463471	1.64	0.28	4.84	0.04	1.00	0.01	1.57	0.02	16200	87
23	LkH$_\alpha$ 233	0.003	0.370	2.01	0.83	1.00	2.39	0.59	5.06	4124	3141
24	LkH$_\alpha$ 314	3.20	0.27	2.99	0.07	8.05	0.30	4.79	0.47	10720	256
25	MC1	9.41	2.63	3.85	0.92	24.21	7.78	24.34	7.31	13940	1936
26	VX Cas	7.78	0.32	3.08	0.05	1.43	0.05	0.94	0.02	12100	135
27	RNO 6	3.32	0.30	5.14	0.12	20.82	1.15	36.30	2.41	16750	279
28	IP Per	0.31	0.63	1.35	0.23	1.00	0.12	0.21	0.04	4360	623
29	XY Per EW	9.62	0.33	2.29	0.05	3.05	0.35	1.12	0.14	9865	162
30	V892 Tau	1.09	0.16	4.51	0.20	14.64	3.92	20.51	6.62	14130	1545
31	UX Ori	5.58	0.24	3.46	0.03	1.00	0.02	0.82	0.016	13020	127
33	P1394	1.00	0.39	3.17	0.08	7.77	0.87	2.20	0.48	5069	318
34	HD 245185	4.30	0.44	2.55	0.10	9.97	0.68	4.84	0.41	9718	269
35	CQ Tau	6.81	0.64	2.18	0.11	4.33	0.51	1.34	0.23	8586	429
37	BD +26887	0.43	0.37	5.49	0.45	1.00	0.00	1.53	0.48	8646	2797
39	LkH$_\alpha$ 215	0.75	0.12	4.66	0.03	1.00	0.09	1.33	0.10	9429	352
40	HD 259431	7.62	0.29	3.36	0.03	1.00	0.03	0.79	0.02	12780	66
42	W121	6.25	0.19	2.64	0.03	1.00	0.00	0.49	0.01	10920	82
43	LkH$_\alpha$ 218	1.74	0.26	4.46	0.04	1.00	0.10	1.35	0.13	15390	122
44	WW Vul	3.16	0.47	2.85	0.11	1.00	0.03	0.67	0.05	10620	366
45	V1685 Cyg	2.55	0.15	7.35	0.27	1.00	0.08	3.52	0.50	21230	307
46	LkH$_\alpha$ 147	3.14	0.27	2.71	0.13	1.00	0.54	0.52	0.27	7971	363
48	BH Cep	3.37	0.45	2.66	0.05	1.00	0.030	0.54	0.02	8409	320
49	BO Cep	0.39	0.15	0.46	0.07	1.00	2.89	0.09	0.56	3698	57
50	SV Cep	6.27	0.41	2.60	0.10	3.06	0.58	1.46	0.58	10800	250

Table 13. SED derived parameters using WISE,2MASS,AKARI data. The parameters are same as in Table 5.

| N0	STAR	DM	EDM	DA	EDA	χ^2	N
1	V633 Cas	-1.00	-1.62	-7.08	-7.09	3.2	38
3	AB Aur	-2.16	-2.59	-6.93	-7.62	2.7	106
5	PQ Tau	-5.60	-3.47	-12.44	-13.13	1.5	57
6	RR Tau	-3.21	-2.92	-8.04	-7.77	0.8	344
7	HD 250550	-2.89	-3.84	-9.15	-8.63	0.9	53
8	LkH$_\alpha$ 208	-4.80	-2.52	-9.91	-8.30	5.0	45
9	LkH$_\alpha$ 338	-1.92	-3.04	-7.70	-8.50	1.5	56
10	LkH$_\alpha$ 339	-1.45	-2.49	-9.29	-9.27	4.7	27
12	V590 Mon	-1.68	-2.25	-5.70	-6.45	2.3	29
13	V360 Mon	-5.02	-3.00	-11.48	-8.61	1.0	126
14	LkH$_\alpha$ 118	-8.04	-2.48	-9.44	-17.72	17.5	3
15	VV Ser	-4.74	-3.73	-9.28	-7.95	1.6	97
16	AS 310 NW	-1.14	-0.61	-7.45	-5.86	41.1	16
17	PX Vul	-5.06	-3.79	-9.76	-8.10	1.9	101
19	LkH$_\alpha$ 324	-7.16	-3.34	-13.95	-9.42	2.3	38
21	LkH$_\alpha$ 234	-1.38	-2.27	-7.31	-8.17	8.4	23
22	BD +463471	-5.03	-3.32	-9.69	-7.80	6.0	125
23	LkH$_\alpha$ 233	-2.75	-1.89	-6.29	-5.95	4.8	13
24	LkH$_\alpha$ 314	-2.40	-2.76	-9.08	-8.76	8.4	65
25	MC1	-3.91	-2.28	-10.14	-6.34	9.0	6
26	VX Cas	-2.78	-3.77	-9.92	-9.340.9	69	
27	RNO 6	-5.47	-2.87	-11.34	-9.49	6.9	52
28	IP Per	-2.28	-2.23	-7.33	-7.40	4.5	29
29	XY Per EW	-2.13	-3.48	-8.36	-9.12	4.8	23
30	V892 Tau	-4.80	-3.97	-9.91	-10.50	25.5	6
31	UX Ori	-3.99	-3.99	-10.57	-9.05	1.3	94
33	P1394	-1.09	-2.21	-7.22	-7.26	4.6	53
34	HD 245185	-1.33	-2.40	-6.95	-7.76	9.1	30
35	CQ Tau	-3.42	-2.57	-9.81	-7.25	5.2	24
37	BD +26887	-2.47	-3.06	-7.94	-8.61	4.1	14
39	LkH$_\alpha$ 215	-3.43	-2.63	-9.61	-8.04	1.7	118
40	HD 259431	-2.16	-2.68	-6.93	-7.57	3.0	94
42	W121	-7.23	-3.35	-13.70	-13.27	3.2	27
43	LkH$_\alpha$ 218	-3.18	-2.87	-8.85	-7.65	1.0	185
44	WW Vul	-3.86	-3.53	-8.82	-9.72	1.1	41
45	V1685 Cyg	-2.95	-2.15	-9.08	-6.71	4.3	63
46	LkH$_\alpha$ 147	-7.10	-3.56	-12.92	-13.08	6.1	24
48	BH Cep	-3.61	-3.56	-9.98	-7.68	2.5	43
49	BO Cep	-1.69	-3.18	-7.88	-8.86	2.6	123
50	SV Cep	-3.16	-3.45	-10.04	-9.07	5.1	26

Fig. 13 shows the variation of disk mass as a function of age. The log(disk mass) is shown in the y-axis. The errors in the estimation of both the parameters are also shown and sources with error less than 20% in disk mass are shown in red. It can be seen that we were able to estimate the disk mass with 20% or less error only for sources with disk mass more than $\sim 10^{-4}$ M$_\odot$. Some of
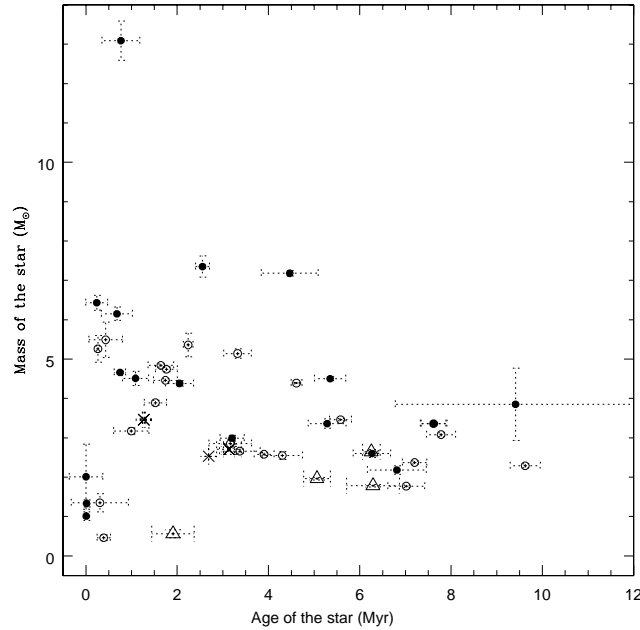
Figure 12. Estimated mass (M$_\odot$) and age (Myr) of HAeBe stars. Class I stars are shown as filled circles, Class II stars are shown as open circles, Class III stars are shown as crosses and Transition Disk sources are shown as triangles. Error in the estimation of mass and age are also shown.

the sources are found to rapidly lose the disk mass such that they have very little disk by 3-4 Myr, which is in tune with the life time of HAeBe stars (Manoj et al. 2006). On the other hand, there are a good number of sources which do not follow this pattern and continue to have relatively large disk mass even at 6-8 Myr. These sources have relatively reliable estimation of disk mass and we observe only a factor of 100 reduction over a time scale of 10 Myr. Hence, there seems to be some mechanism by which some of the stars continue to keep the disk for longer duration. This result, which is suggestive from this study needs to be confirmed.

In Fig. 14, we have shown the variation of disk accretion rate as a function of age. Similar to Fig. 13, sources with error less than 20% in the accretion rate are shown in red. Here also, we can visualise a similar group with rapidly decreasing disk accretion rate with age such that there is negligible accretion by 3-4 Myr. Some of these sources have relatively better estimation of the accretion rate to support the above arguement. These sources are found to be same as those found in Fig. 13, which have reduced disk mass. Also, a set of sources are found to carry on with a relatively high accretion rate for older ages also. Thus, once again, our study is indicates that there could be a mechanism to sustain disk accretion even at older ages. We find that some of the Class I stars are very young, with large disk mass and large accretion rate, whereas the Class II stars are relatively older with lesser disk mass and accretion rate, followed by Class III sources of
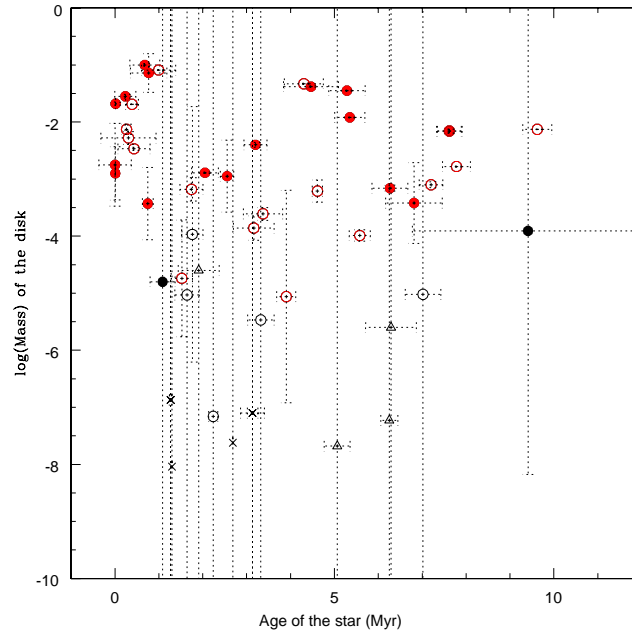
Figure 13. Disk mass ($M_\odot$) is shown as a function age (Myr) for the HAeBe stars. The details are same as in Fig. 12. The error in the estimation are also shown. Sources with error less than 20% in disk mass are shown in red.

3-4 Myr, where there is negligible disk present. The sub-class with the above properties seem to tentatively indicate an evolutionary progression from Class I to II to III. We are unable to confirm this due to large error in the estimation of the disk mass, especially for stars with low disk mass.

In order to understand the dependence on the mass of the star, we have plotted the disk mass with respect to mass of the source in Fig. 15. The plot shows that sources with a range in mass show similar accretion rate. Also, as seen in the case of Fig. 13, we were able to estimate the disk mass with 20% or less error only for sources with disk mass more than $\sim 10^{-4}$ $M_\odot$. In the case of sources with disk mass more than the above value, we observe a range in disk mass even for sources with similar mass. In Fig. 16, we show the dependence of accretion rate with mass of the star. We observe that sources with similar mass are found to have a range in the accretion rate.

The correlation found in Figures 13 and 14 suggest that there may be a relation between disk accretion rate and disk mass, which we explore in Fig. 17. A similar attempt to compare this relation between HAeBe stars and T-Tauri stars was done by Mendigutía et al. (2012). As these stars are located in various environments, it will be interesting to see whether this is an intrinsic property. The plot has a large range in disk accretion and disk mass, as the axes are shown in log scale. Sources with 20% or less error in one of the two parameters plotted are shown in red.
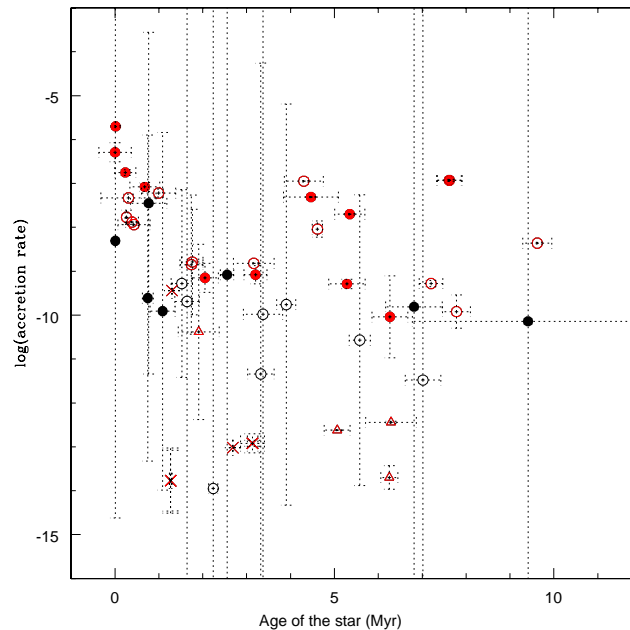
Figure 14. Disk Accretion rate ($M_\odot$/year) as a function of age (Myr) for the HAeBe stars. The details are same as in Fig. 12. Sources with error less than 20% in accretion are shown in red.

Sources with large disk mass have relatively small errors in both values, but sources with less accretion rate (and shown in red) have large errors in disk mass. A linear fit to the data (except one source) is also shown in the figure. The correlation coefficient suggests the fit to be reasonably good. The estimated coefficients and their errors are also shown in the figure. A similar plot was generated by Mendigutía et al. (2012) (their figure 6) and the estimated coefficients are found to be very similar. The interesting point to notice is that sources which are suggested to lose their disk rapidly and those which are suggested to retain disks for longer time show similar relation between disk mass and disk accretion rate.

In this study we have used homogeneous data over a large range of wavelength to classify 50 HAeBe stars. We have performed classification based on two methods and are able to classify previously unclassified objects. The SED analysis is done using a web tool and the parameters are estimated for all the stars. The analysis performed shows that we are able to understand the evolution of these sources as a function of age as well as derive correlations. Deviations in the parameters derived here from the literature values could be due to the difference in models used to model the SEDs. In summary, the analysis performed in this study demonstrates its potential to study more stars in this category. The study also suggests that coverage of data over a larger range of wavelength including FIR will improve the estimation of SEDs as well as the derived parameters. This is also necessary to confirm the results suggested by this study.
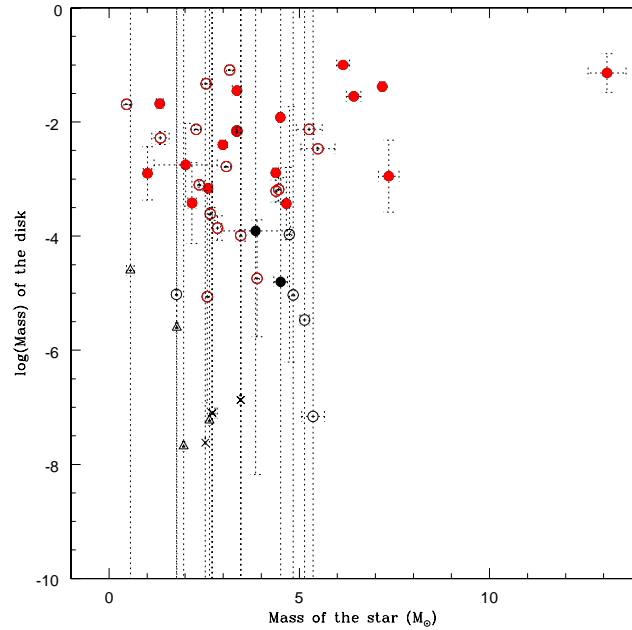
Figure 15. Disk mass (M$_\odot$) is shown as a function mass (M$_\odot$) for the HAeBe stars. The details are same as in Fig. 12. The error in the estimation are also shown. Sources with error less than 20% in disk mass are shown in red.

7.   Conclusions

We list out the results and conclusions of this study.

- We present the classification and study of disk parameters of 50 Herbg Ae/Be stars using AKARI, WISE and 2MASS and visual data. These stars have been classified into 4 groups based on the scheme proposed by Koenig et al. (2012) using WISE pass bands and by constructing SEDs using data up to 12 pass bands.

- We could successfully classify 50 sources into 4 groups, of which 18 are classified for the first time, using WISE color-color diagrams and SEDs. We classified 18 sources as Class I, 22 sources as Class II, 6 sources as Class III and 4 sources with Transitional Disk. Thus, we have achieved classification of about one third of the sample for the first time.

- SEDs created with and without AKARI data were found to be similar for a good fraction of sources, though some sources showed large deviation. This may be due to the large PSF of the AKARI data. Stellar and disk parameters of 50 sources were estimated from SEDs and correlation between various parameters are studied. Due to large errors, the results derived in this study are only indicative.
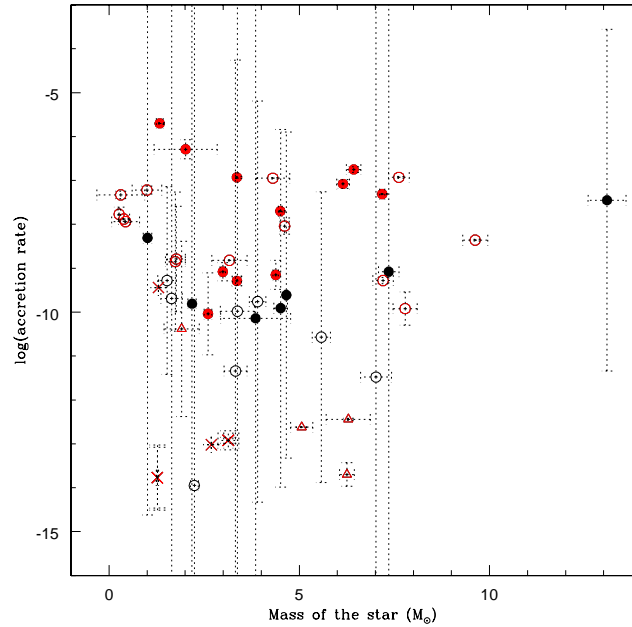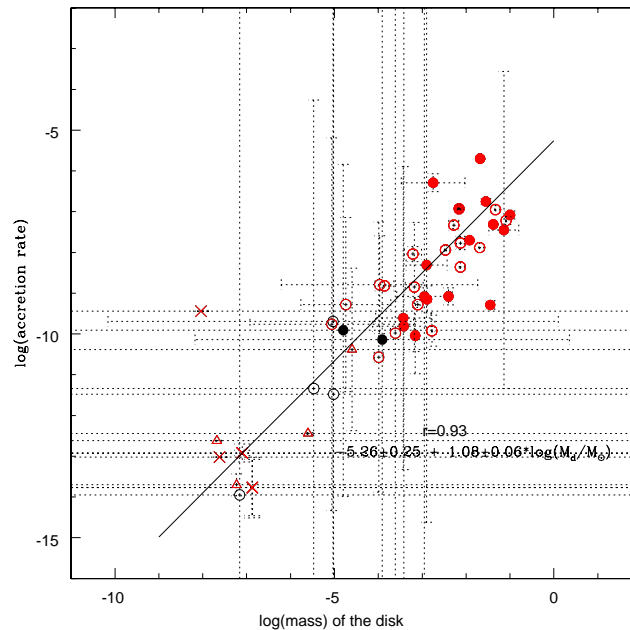
Figure 16. Disk Accretion rate ($M_\odot$/year) as a function of mass ($M_\odot$) for the HAeBe stars. The details are same as in Fig. 12. Sources with error less than 20% in accretion are shown in red.

- Analysis of the present sample tentatively suggests that sources more massive than ~ 6 $M_\odot$ may have a very short Class II phase, whereas stars in the mass range 2-5 $M_\odot$ spend relatively long time in the Class II phase.

- Among the present sample, this study tentatively suggests the following trend - when one set of stars are found to lose their disk rapidly such that they have negligible disk mass as well as disk accretion rate when they are 3-4 Myr old. This sub-group is suggestive of a progression of evolution from Class I to II to III with age, though the result is only indicative due to large errors.

- This study also tentatively suggests another set of sources which retain their disk as well as accretion till 6-8 Myr, indicative of a mechanism by which some of the stars continue to keep the disk for longer duration.

Acknowledgments

Figure 17. Correlation between disk mass ($M_\odot$) and disk accretion rate ($M_\odot$/year) for HAeBe stars. A straight line fit to the data points, excluding star 16, is also shown. The details are same as in Fig. 12. Sources with less than 20% error either in disk mass or accretion rate are shown in red.

References

Acke B., van den Ancker M. E., 2006, A&A, 457, 171
Alexander R. D., Armitage P. J., 2009, ApJ, 704, 989
Andrews S. M., Wilner D. J., Espaillat C., et al., 2011, ApJ, 732, 42
Calvet, N., DAlessio, P., Watson, D. M., et al. 2005, ApJ, 630, L185
D'Alessio P., Hartmann L., Calvet N., et al., 2005, ApJ, 621, 461
Finkenzeller U., Mundt R., 1984, A&AS, 55, 109
Fuente A, Martín Pintado A., Bachiller R., Rodríguez-Franco A., Palla F., 2002, A&A, 387, 977
Greene T. P., Wilking B. A., Andre P., Young E. T., Lada C. J., 1994, ApJ, 434, 614

Hajjar R., Bastien P., 2000, ApJ, 531, 494

Herbig G. H., Bell K. R., 1988, Third catalog of emission-line stars of the Orion population., Lick Observatory Bulletin 1111, Santa Cruz: Lick Observatory, p. 90

Herbig G. H., 1960, ApJS, 4, 337

Hernandez J., Calvet N., Briceno C., Hartmann Lee, Berlind P., 2004, AJ, 127, 1682

Hillenbrand L. A., Stephen E., Strom, Frederick J., Vrba, Joccelyn Keene, 1992, ApJ, 397, 613

Huang Y. F., Zeng L. J., Rector T. A., Mallamaci C. C., 2013, AJ, 145, 126H

Jarrett et al., 2011, ApJ, 735, 112

Juhász A., Bouwman J., Th., Henning, Acke B., Van den Ancker M. E., Meeus G., Dominik C., Min M., Tielens A. G. G. M., Waters L. B. F. M., 2010, ApJ, 721, 431

Koenig X. P., Leisawitz D. T., Benford D. J., Rebull L. M., Padgett D. L., Assef R. J., 2012, ApJ, 744, 130

Lada C. J., 1987, in Peimbert M., Jugaku J., eds, Proc. IAU Symp. 115, Star Forming Regions (Cambridge: Cambridge Univ. Press), 1

Maheswar G., Manoj P., Bhatt H. C., 2002, A&A, 387, 1003

Mendigutía I., Mora A., Montesinos B., Eiroa1 C., Meeus G., Mern B., Oudmaijer R. D., 2012, A&A, 543, 59

Manoj P., Bhatt H. C., Maheswar G., Muneer S., ApJ, 653, 657

Pott J.-U., Perrin M. D., Furlan E., et al., 2010, ApJ, 710, 265

Robitaille T. P., Whitney B. A., Indebetouw R., Wood K., Denzmore P., 2006, ApJSS, 167, 256

Robitaille T. P., Whitney B. A., Indebetouw R., Wood K., 2007, ApJSS, 169, 328

Strom K. M., Strom S. E., Edwards S., Cabrit S., Skrutskie M. F., 1989, AJ, 97, 1451

Thé P. S., de Winter D., Pérez M. R., 1994, A&A SS, 104, 315

van den Ancker M. E., Thé P. S., Feinstein A., Vazquez R. A., de Winter D., Perez M. R., 1997, A&AS, 123, 63

Verhoeff A. P., Waters L. B. F. M., Van den Ancker M. E., Min M., Stap F. A., Pantin E., Van Boekel R., Acke B., Tielens A. G. G. M., de Koter A., 2012, A&A, 538, 101

Waters L. B. F. M., Waelkens C., 1998, ARAA, 538, 101

Wright et al., 2010, AJ, 140, 1868

Yamamura et al., 2010, AKARI Bright star catalog